JOSHUA

The Journal of Science and Health at the University of Alabama

2017

Volume 14

About the Cover:

Drosophila melanogaster is a species of fruit fly commonly used for experimental purposes. The organism is particularly useful for examining aging and immunity as it is easily cultured, is genetically tractable, and has a relatively short lifespan. This picture was taken by Dr. Kim Lackey on a scanning electron microscope for the Chtarbanova Lab at the University of Alabama.

2016-2017 JOSHUA Staff

Questions should be directed to joshua.alabama@gmail.com, and more information and all archived volumes are available at joshua.ua.edu.

Table of Contents

High-Throughput Selection for High Producing CHO Clones Using Fluorescence-Activated Cell Sorting

Kyle Leonard ……..…….……...……..……..…...**4**

Establishing a co-culture system for *Clostridium cellulovorans* and *Clostridium aceticum* for high efficiency biomass transformation

Donna Xia ……...……...…….…..…..**8**

Investigation of the intersection of cholesterol metabolism, neurodegeneration and lifespan in a C. elegans model of Parkinson's Disease

Samantha Glukhova……..……..…..…..**14**

A Review of the Molecular Basis for Nicotine Addiction

Brian Smithers…… …….……...…..……..**18**

Isolation and Characterization of *Staphylococcus epidermidis* bacteriophage

Madeleine Hull, Steven Scaglione…….…….…….…….…….**23**

Role of miRNA in Dopamine Synthesis and Signaling

Samuel Stanley……..……...…….…….…….…….**32**

Emerging Scholars Abstracts

Emerging Scholars…….**36**

Interview with Stanislava Chtarbanova-Rudloff

JOSHUA…….……..…..**38**

High-Throughput Selection for High Producing CHO Clones Using

Kyle Leonard [1] , Mary Taglieri [1] , Michael Burnette [1] , Kelley Cooper [1] , Graham Grogan [1] , Lauren Pan [1] , Joanna Urli [1] , Ningning Xu [1] , and Margaret Liu [1]

Faculty Mentor: Margaret Liu

[1]*Department of Chemical and Biological Engineering, The University of Alabama, Tuscaloosa, Alabama 35487*

Selection of high-producing clones is critical to ultimately developing an efficient Chinese Hamster Ovary (CHO) platform for industrial monoclonal antibody (mAb) production. However, high producers are extremely rare and a large number of cells must be screened to identify the desirable clones [5]. This project utilized the accuracy and precision of Fluorescence-activated cell sorting (FACS) to efficiently sort successfully transfected CHO cells based on the expression level of recombinant proteins. Fluorescein isothiocyanate (FITC) - conjugated Goat Anti-human IgG (H&L) labeled the secreted IgG proteins that remained on the surface of CHO cells at low temperature. Then, the stained cells were analyzed and confirmed using confocal microscopy, and the S3e Cell Sorter was utilized to isolate high-producing CHO clones from a CHO DG44/IgG cell pool. The developed FACS-based method can screen a large number of clones with superior productivity in a short time, which accelerates the CHO cell line development for therapeutic protein production.

Introduction

Recombinant proteins and monoclonal antibodies have played a critical role in the biopharmaceuticals market, and the demand for new recombinant proteins and antibodies is anticipated to increase [2,11]. Thus, efficient and robust processes are needed to meet the growing number of new recombinant proteins and antibodies. To optimize the production of mAb's, this project considers Chinese Hamster Ovary (CHO) cells as a possible platform to produce biopharmaceuticals. CHO cells are some of the most widely used mammalian cell platforms for synthesizing human-compatible drugs in the biopharmaceutical industry. This is due to the cells' viability at high densities in bioreactors, regulation of post-translational modification of proteins, and their relative ease of adaptability from adherent growth to serum-free suspension [3,5,9]. Furthermore, CHO cells contain a versatile genetic structure that allows for smooth transfection of select gene vectors into their genome to produce a wide variety of proteins [10]. This versatility, along with their demonstrated safety as recombinant hosts, has made a positive impression on regulatory agencies resulting in faster administrative approval, which leads to a shorter wait for available clinical treatments [4]. By manipulating these special characteristics, CHO cells can be genetically engineered to produce recombinant proteins through transfection with a genetic vector containing the gene of interest. Once the CHO cells have been transfected with this gene of interest to produce the desired recombinant protein, they are subject to selection, amplification, and cloning to obtain an improved protein titer.

Selection of high-producing clones is imperative to ultimately developing an efficient platform for industrial mAb production. However, isolation of high producing clones from a cell pool remains a bottleneck in the timeline of cell line development. The conventional cloning method is limiting dilution screening, in which single cells are analyzed for their protein titration and clonal expansion. As this method is laborious and limited in the quantity of cells screened, there is a high likelihood of missing the highest producing clones. Consequently, high-throughput methods have recently been developed to efficiently screen clones from cell pools, such as fluorescence-activated cell sorting. In this method, the specific productivity of a clone is evaluated by a fluorescent signal, the ClonePix FL, in which individual colonies are formed from single cells in a semi-solid media, ranking the clones by their exterior fluorescent intensity.

In this study, confocal microscopy was used to visualize and confirm florescence-labeled antibody-producing CHO cells, while fluorescence-activated cell sorting was applied to enrich the sub-population of high-level antibody producing CHO cell clones. Laser scanning confocal microscopy (LSCM) is a fluorescence-sensitive microscopy method that has been used in various fields of biological research, including analysis of cell-cell communication and chromosomal analysis [6]. LSCM can also be used to generate three-dimensional images from a series of two-dimensional cross sectional images taken in a short time lapse. The three-dimensional constructs can then be modified and adjusted to evaluate the resulting distribution of fluorescent particles within the sample analyzed.

Fluorescence-activated cell sorting (FACS) is a specialized method of flow cytometry used to sort cells based on fluorescent character expressed on the cell surface [1,5]. Fluorescent-conjugated antibodies label the secreted recombinant proteins that remain on the surface of cells at low temperature, while high producer cell clones are determined by the fluorescence signal [5,7]. Specifically, FACS channels the solution into a single-file line of droplets containing individual cells through a laser beam, which applies a charge to droplets containing fluorescence-labelled cells. The charged droplets then pass through an electric field formed by charged deflector plates to deviate from the uncharged droplets and be collected together in a tube. Thus, the high- producing clones are isolated from the rest of the solution.

Materials and Methods

Cell Culture, Transfection, and Amplification

Chinese Hamster Ovary cells (CHO DG44) (Thermo Fisher Scientific) were cultured in CD DG44 (Gibco) supplemented with 8 mM L-glutamine, H/T, and Pluronic F-68 (Gibco) prior to transfection, and grown in CD FortiCHO supplemented with 8 mM L-glutamine post-transfection. The cells were matured in shaker flasks and incubated at 37°C, 5% CO 2 . FreeStyle MAX reagent was used to transfect CHO DG44 cells with two plasmids encoding antibody light chain and heavy chain. The stably transfected CHO DG44/IgG cell pools were selected in H/T deficient medium with G418, and subsequently amplified by MTX to improve the recombinant protein expression. ELISA was used to determine the protein titers of each CHO/IgG cell pool.

Cell Staining and Confocal Microscopy

The amplified CHO DG44/IgG cell pools were thawed and cultured for either seven or ten days prior to taking confocal images and sorting cells. To prepare the stained CHO DG44/IgG cell samples, a total of 5x10 6 cells were centrifuged at 200xg, at 4°C for 3 minutes. The cell pellets were washed with 4°C PBS Buffer, centrifuged again, and re-suspended with 1 mL of cold PBS buffer. For the cell staining, 100 uL fluorescein isothiocyanate (FITC) - conjugated Goat Anti-human IgG (H&L) (0.5 ug/uL) (KPL) was added to the cells, and subsequently incubated for 30 minutes on ice. The cell samples were washed once with cold PBS buffer, re-suspended with cold PBS buffer, and incubated on ice until confocal imaging and cell sorting. A stained, non-transfected, negative control was prepared with an identical protocol. The stained cell samples were placed in 35 mm glass bottom dishes and mounted on the stage of a confocal microscope (Nikon) with a 60x oil immersion objective lens (Nikon) to visualize cells. Laser excitation light was provided at a wavelength of 495 nm, and fluorescent emissions were collected at wavelengths of 519 nm.

Cell Sorting and Limiting Dilution Cloning

The stained cell samples were sorted on S3e Cell Sorter (Bio-Rad) using a laser emitting at 488 nm and detecting FITC emission with a 525/30 filter. Before using the sorter, the fluid containers in the machine were checked to ensure they were at the appropriate level and the waste container was emptied. The cell sorter machine was cleaned and sterilized with sterile water and sheath fluid and then calibrated using calibration beads. The sort gate was sensitive only to cells with the top 5% fluorescence (from the FITC histograms); the sorted cells were deposited into 5 mL Falcon tubes containing CD FortiCHO medium supplemented with L-glutamine.

The collected high producing CHO DG44/IgG cells were counted using hemacytometry and serially diluted with cloning medium until a final cell density of 5 cells/mL was obtained. Then, 200 uL aliquots of the diluted cell culture were dispensed using a multiple-channel pipette into a 96-well plate (Corning). The seeded cells were incubated at 37°C, 5% CO 2 for ten days, where fresh medium was added into the wells on day 7. ELISA was utilized to once again screen the surviving cells, and the top 10 clones were gradually scaled up until they were in shaker flasks [8]. Finally, cell growth profiles and protein titers of the clones were assessed to identify the most efficient clone of CHO DG44/IgG.

Results and Discussion

Labeling Recombinant IgG with Product-Specific Fluorescence

After transfection and amplification, CHO cells secreting recombinant proteins can be directly stained with fluorescently labeled antibodies. The secreted recombinant proteins would be stuck on the surface of the CHO cells at low temperature. In binding fluorescence to the specific recombinant proteins, confocal microscopy illuminated the fluorescing proteins to be imaged (Figure 1). The confocal microscope shows a three-dimensional image of the shell along with a cross section and a shell with reduced axes to demonstrate that the fluorescing proteins are located only on the cell membrane. Demonstrating that the proteins are only on the outside of the cell is significant because it substantiates the claim that the

proteins of interest are secreted from the cell after production. This is important as secreted biopharmaceutical proteins are easier to harvest and separate from the production medium than proteins that are produced and remain in the cell. The images confirm that the recombinant secreted IgG protein can be directly stained on the CHO cell surface. As the amount of secreted recombinant proteins remaining on the cell surface correlated with the total amount of proteins being secreted from the cells, this product-specific staining can be used as the basis for cell sorting.

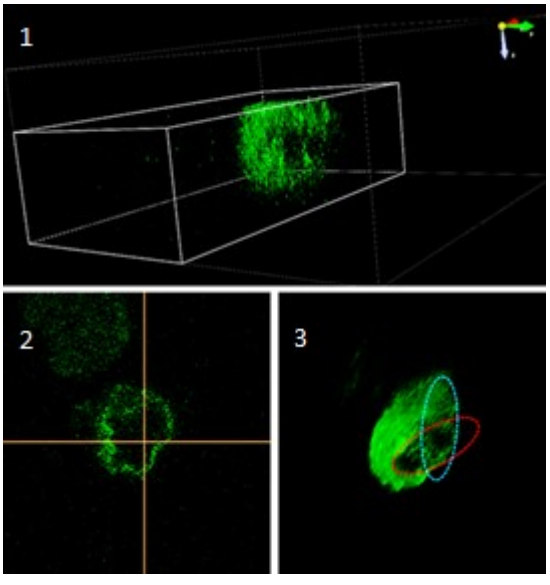

Figure 1: Confocal imaging shown in three views. Three-dimensional depiction of an antibody producing CHO cell with axes labeled (1). Cross-section of the CHO DG44/IgG cell showing the extracellular concentration of fluorescent proteins (2). Three-dimensional shell of the cell with reduced y-axis in blue and reduced z-axis in red (3).

Sorting Enriches Sub-populations of CHO DG44/IgG with High Expression

The stained, non-transfected CHO host cells and stained CHO DG44/IgG cells were separately analyzed by the S3e Cell Sorter in a cycle model (Figure 2). Populations of cell samples with fluorescence intensity exceeding that of negative control were accounted for during cell sorting.

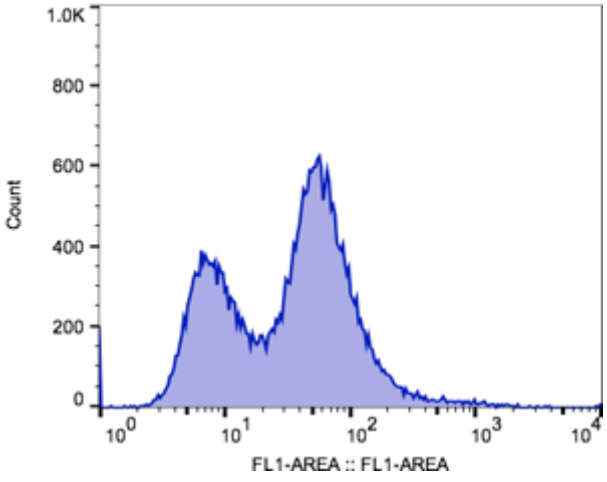

Figure 2: Fluorescence distribution in stained negative control and stained CHO DG44/IgG cells. FL1, fluorescence intensity; count, cell number. The peak on the left shows the stained non-transfected host negative control, the peak on the right shows the stained CHO DG44/IgG cell.

Conclusion

This project developed a FACS-based screening method for the isolation of high antibody-producing clones from a transfected cell pool. The CHO DG44/IgG cells labeled with fluorescein isothiocyanate (FITC)-conjugated Goat Anti-human IgG (H&L) were enriched via utilizing the S3e cell sorter and subsequently visualized by confocal microscopy, confirming the results of the S3e Cell Sorter. This FACS-based high throughput screening method enables efficient selection of high-producing clones, furthering the development of a CHO cell line capable of efficiently producing mAbs. This efficient production will allow for lower production costs and ultimately lower treatment costs. However, the ideal choice of mAb to produce using this platform is still relatively unexplored.

References

[1] Aebisher D, Bartusik D & Tabarkiewicz J. (2017). Laser flow cytometry as a tool for the advancement of clinical medicine. Biomedicine & Pharmacotherapy, 85:434-443.

[2] Aggarwal RS. (2014). What's fueling the biotech engine-2012 to 2013. Nat Biotechnol, 32:32–39.

[3] Cacciatorea JJ, Chasin LA & Leonard EF. (2010). Gene amplification and vector engineering to achieve rapid and high-level therapeutic protein production using the Dhfr-based CHO cell selection system. Biotech. Adv, 28:673–681.

[4] Kim JY, Kim YG & Lee GM. (2012). CHO cells in biotechnology for production of recombinant proteins: current state and further potential. Applied Microbiology & Biotechnology, 93(3):917-930.

[5] Lai T, Yang Y, Ng SK. (2013). Advances in mammalian cell line development technologies for recombinant protein production. Pharmaceuticals, 6 (5):579-603.

[6] Singh A & Gopinathan KP. (1998). Confocal microscopy: A powerful tool for biological research. Biology Faculty Publications, 74:841-851.

[7] Tomlinson MJ, Tomlinson S, Yang BY & Kirkham J. (2013). Cell separation: Terminology and practical considerations. Journal Of Tissue Engineering, 4:1.

[8] Urli J, Borcky T, Cooper K, James J, Leonard K, Panian J, Taglieri M, Xu N & Liu M. (2016). Characterization of IgG1 antibodies expressed in CHO cells by ELISA and RP-HPLC. The Journal of Science and Health and the University of Alabama, 13:4-7.

[9] Xu N, Ou J, Gilani A, Zhou L & Liu M. (2015). High-level expression of recombinant IgG1 by CHO K1 platform. Frontiers of Chemical Science and Engineering, 9(3): 376-380.

[10] Xu N, Ma C, Sun W, Wu Y, & Liu XM. (2015). Achievements and perspectives in Chinese hamster ovary host cell engineering. Pharmaceutical Bioprocessing, 3(4): 285-92.

[11] Zhou L, Xu N, Sun Y & Liu XM. (2014). Targeted biopharmaceuticals for cancer treatment. Cancer Letters, 352(2):145-151.

Acknowledgements

This work was supported by the Research Grant Committee (RGC), a grant from the Department of Chemical and Biological Engineering, and funding by the National Science Foundation (BRIGE 24512).

About the Authors

Kyle Leonard is a junior from Troy, Michigan studying chemical engineering with a minor in biology at the University of Alabama and plans to attend medical school. He has worked in Dr. Margaret Liu's lab for a year and a half and presented his research at the American Institute of Chemical Engineers Southern Regional Conference and the Undergraduate Research and Creative Activity Conference in Tuscaloosa, Alabama in March 2016. He is very thankful for the support of Ningning Xu and Dr. Liu during his time working in the lab.

Mary Taglieri is a junior from York, Pennsylvania working towards a dual degree in chemical engineering and chemistry at the University of Alabama with the goal of attending medical school or pursuing biopharmaceutical research. During the year and a half she has worked in Dr. Margaret Liu's lab, she has presented research at the American Institute of Chemical Engineers Southern Regional Conference and the Undergraduate Research and Creative Activity Conference in Tuscaloosa, Alabama in March 2016. She is grateful for the mentorship from Ningning Xu and Dr. Liu.

Establishing a co-culture system for *Clostridium cellulovorans* and *Clostridium aceticum* for high efficiency biomass transformation

Donna Xia[1], Ann Kay Alexander[1], Alisha Isbell[1], Shuyuan Zhang[1], Jianfa Ou[1], X. Margaret Liu[1]

Faculty Mentor: Margaret Liu

Department of Chemical and Biological Engineering, The University of Alabama, Tuscaloosa, AL 35487

C4 bio-refinery, such as butyrate and butanol production, is currently a research hotspot. However, undesirable waste products including H_2 and CO_2 result in lower product yield and energy waste. Clostridium aceticum has the ability to convert H_2 and CO_2 to acetate, which can be assimilated by other Clostridia strains through the reversible acetate kinase and phosphotransacetylase pathway. This study set up a co-cultural system for C. aceticum and C. cellulovorans. Together they can convert the cellulosic biomass to butyrate or even butanol if a metabolically engineered strain is used, with considerably higher yields. Based on DSMZ 520 medium for C. cellulovorans and DSMZ 135 acetobacterium medium for C. aceticum, the practical pH ranges were evaluated for both strains. The pH 7.0-7.5 was suitable for both strains. By mixing these media with various ratios, an optimized formulation was defined for the co-cultural system.

Introduction

Due to its high energy content, compatibility with current combustion engines, and blending ability, biobutanol is a promising alternative fuel source to gasoline. Furthermore, new metabolic pathways are being discovered that will cut back the amount of hydrogen gas (H_2) and carbon dioxide (CO_2) released into the atmosphere to almost zero. Despite these advantages, biobutanol is more expensive to produce and production is hindered by the high costs. Fortunately, however, there is promise that a co-culture between two microorganisms could potentially biorefine biomass to create a high-value product, thereby reducing the costs of biobutanol production.

Butanol can be formed by via fermentation through biological conversion of lignocellulosic biomass. Previous studies have encouraged the usage of bacteria in the Clostridium genus. *Clostridium cellulovorans* was selected as the primary bacterium as it showed significant potential for an economical butanol production along with possessing unique gene pathways. *C. cellulovorans* is an anaerobic, Gram-negative, mesophilic, spore-forming cellulolytic bacterium. *C. cellulovorans* has a large number of cellusomal genes and can efficiently degrade plant cell wall polysaccharides [4]. Furthermore, *C. cellulovorans* requires only one heterologous gene, adhE2, to enable biobutanol production from butyrate.

Although butyric acid is the main metabolic product from butyryl-CoA, a minimal amount of acetic acid, CO_2 and H_2 are produced as byproducts. *C. cellulovorans* can assimilate acetate to generate acetyl -CoA and use it to produce butyrate. Studies have shown that H_2 and CO_2 can be converted to butyric acid through gaseous substrate reaction with several potent species of bacteria, one of which is *Clostridium aceticum* [1]. *C. aceticum* is a homoacetogen that grows chemolithotrophically with H_2 and CO_2 and achieves product yield stoichiometrically using the Wood-Ljungdahl pathway as seen in the following reaction:

$$2CO_2 + 4H_2 \rightarrow CH_3COOH + 2H_2O$$

With high yield, high titer, and high productivity compared to glucose, *C. aceticum* pathways suggest a high metabolic flux from CO_2 to acetyl-CoA [3]. Despite the possibility of higher substrate utilization efficiency, a co-culture between *C. aceticum* with *C. cellulovorans* has not been established yet. Previous co-culture systems combined biomass substrate with *C. cellulovorans* in order to improve the theoretical yield of butyrate for a more economical system [2]. A metabolic pathway between the two microorganisms is illustrated in Fig. 1, where the proposed recycle pathway can be seen as *C. aceticum* takes the undesired waste products and converts them into acetate. It is expected that this co-culture will increase the yield of both acetate and butyrate while reducing the waste of carbon.

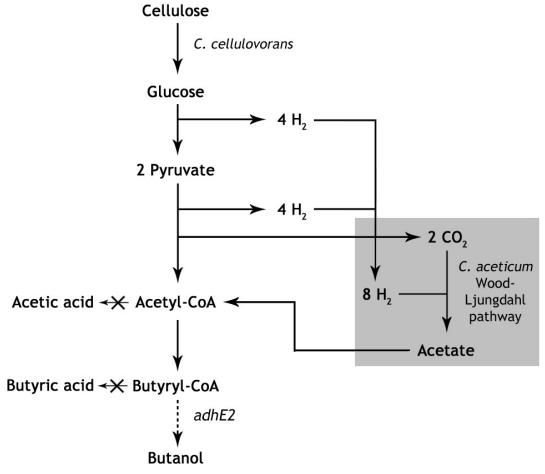

Figure 1. Proposed metabolic pathway for *C. cellulovorans* and *C. aceticum* using the Wood-Ljundahl pathway to produce acetate that can be assimilated by *C. cellulovorans* to generate to acetyl-CoA.

The goals of this study were to create a viable co-culture system while identifying both an optimal pH and medium formulation for both strains of bacteria and to focus specifically on identifying *C. aceticum*'s viability to co-exist with *C. cellulovorans.* Current results from previous studies conducted by the lab show that *C. aceticum* can survive a pH as low as 7.0 while *C. cellulovorans* can survive a range between 7.0-7.5. However, the substrate yield and the pH are positively correlated, potentially pointing to a high final pH for this experiment. Additionally, a ratio between two mediums must be decided. *C. aceticum* and *C. cellulvorans* require a specific type of medium in order for the microorganism to grow effectively. This co-culture will need an optimal medium ratio in order to maximize the amount of cells that can work through the pathway.

Methods and Materials

A serum bottle culture was used to determine the optimized formulations. Free-cell fermentation was performed with 45 mL of medium in serum bottles that were stored in an incubator at 37°C. Sampling occurred daily and stopped after 6 to 7 days as the concentration of bacterial cells declined. Cell density was monitored using a spectrophotometer (OD_{600}) while concentrations of butyrate and acetate were analyzed using high performance liquid chromatography (HPLC). For the pH optimization formulation, five different values of pH were tested and compared: 7.0, 7.5, 8.3, 9.0, and 9.5. The medium ratio optimization tested five ratios; 1:1, 1:4, 2:3, 3:2, 4:1 (DSMZ 520:DSMZ 135).

Serum Bottle Culture:

2.1 Serum Bottle Culture:

DSMZ 135	
Component	Amount Needed
NH_4Cl	1.0 g
KH_2PO_4	0.33 g
K_2HPO_4	0.45 g
$MgSO_4$	0.025 g
Yeast Extract	2.0 g
L-Cysteine $HClH_2O$	20 mL
Trace Element Solution (5/17/2016)	20 mL

Table 1. DSMZ 135 Acetobacterium medium for C. *aceticum*. The components were first dissolved in 500 mL deionized H2O. The pH was adjusted to 7.5 and final volume adjusted to 900 mL .

DSMZ 520	
Component	Amount Needed
$(NH_4)_2SO_4$	1.3 g
KH_2PO_4	3.3 g
$MgCl_26H_2O$	0.2 g
Yeast Extract	2.0 g
Tryptone	4.0 g
Cysteine HCl	0.5 g
Modified Trace Element (1000x, 2/23/2016)	1.0 mL
$CaCl_2$(10 g/L)	7.5 mL
$MnSO_4$(10,000x)	50 µL

Table 2. DSMZ 520 medium for C. *cellulovorans*. The components were first dissolved in 700 mL deionized H2O.The pH was adjusted to 7.5 and final volume adjusted to 900 mL .

C. cellulovorans and *C. aceticum* were each grown in the liquid mediums DSMZ 520 and DSMZ 135, respectively, composed of the elements shown in tables 1 and 2. Prior to sterilization, each serum bottle was filled with 45 mL of specified DSMZ medium using the formulation shown in (table) and deionized water (ddH_2O). For the pH optimization formulation, after the medium was thoroughly dissolved, the pH was then adjusted to five different pH values for comparison by using 2.0 M NaOH or 2.0 M HCl: 7.0, 7.5, 8.3, 9.0, and 9.5. For the medium ratio optimization, DSMZ 520 and DSMZ 135 were mixed at the following ratios: 1:1, 1:4, 2:3, 3:2, 4:1 (DSMZ 520:DSMZ 135) to equal 45 mL total volume per serum bottle. Once the medium was adjusted to the appropriate pH or medium ratio, the medium went through dissolved oxygen removal by vacuum degassing in an anaerobic chamber. Nitrogen gas was allowed to enter the chamber five times to ensure that the medium could be degassed of oxygen. The serum bottles were sealed with gas impermeable butyl rubber septum-type stoppers and aluminum crimp seals in the chamber. The bottles were then sterilized further in an autoclave for 45 minutes at 120°C. The serum bottles were at 37°C after inoculation. Samples were extracted by sterilized syringes daily until the concentration of the bacterial cells declined. These samples were used for testing the optical density (OD_{600}) as well as analyzation through high performance liquid chromatography (HPLC). OD samples were extracted directly from the serum bottles whereas the HPLC samples were centrifuged for 10 minutes at 10,000 rpm followed by 0.22μm filtration, using the supernatant as the sample. The biomass pellet was disposed.

Before inoculation, the work environment was sterilized using a spray consisting of 70% ethanol and was allowed to air dry. A bunsen burner was turned on to ensure the continuation of a sterile environment. The aluminum crimp seal and butyl rubber septum-type stoppers of each serum bottle were sprayed with the same ethanol spray and held over the flame. Using an autoclaved syringe, 5 mL of the bacteria strain was introduced into each serum bottle. Vitamin solution and fructose solution were added at the same time. Once inoculated, the tops of the bottles were sprayed and put into an incubator kept at a constant temperature of 37°C.

Analytical Methods

Spectrophotometer to monitor cell concentration

The cell concentration was monitored daily by using a spectrophotometer to test the optical density (OD_{600}) of the sample liquid. Monitoring the cell density daily allowed for a close watch on when the growth of the bacterial cells began to decline, which was found to be 6 to 7 days. The resulting value of the optical density was then compared to a standard curve for the absorbance of either C. *cellulovorans* or C. *aceticum*.

High Performance Liquid Chromatography (HPLC) Analysis

HPLC is a separation technique where the sample is injected into a tube that is packed with porous particles and uses high pressure to transport the sample through the tube in eluent, which was HPLC-grade H_2O, at a flow rate of 0.6 mL/min. During the process, the use of chemical and physical interactions (such as polarity) are implemented to separate individual components from the original sample. The sample liquid was centrifuged and the supernatant was used for analysis of acetate concentration and consumed fructose. The HPLC system in this experiment was equipped with an automatic sampler, which measures the appropriate volume for the sample, injects the sample, and then flushes the system to prepare for the next vial. 45 microliter samples were micro pipetted into the cleaned sample vials and loaded into the automatic sampler. The automatic sampler continued its process until all samples were complete. The HPLC was also equipped with a solvent delivery unit, an organic acid and solvent analysis column, and a column oven that reached 78°C. A refractive index detector, which measures the ability of particles in a sample to deflect light, was also included. In this experiment, the amount of deflected light was proportional to the concentration of the particular molecule being tested for, either acetate or glucose.

pH Optimization

Previous studies have shown that *C. cellulovorans* can survive in a pH range between 7.0-7.5, so five pHs (pH 7.0, 7.5, 8.3, 9.0, and 9.5) were tested in order to determine which was best for C. *aceticum* growth. The DSMZ 135 medium was separated and then adjusted to the corresponding pH with 2.0 M HCl or 2.0 M NaOH, depending on the initial pH. Once the pH was adjusted, the medium's volume was adjusted accordingly and separated into labeled glass serum bottles. Samples were taken daily to monitor cell density. The purpose of this portion of the experiment was to find an optimal pH for both C. *cellulovorans* and C. a*ceticum* in order to create a successful co-culture system

Medium Ratio Optimization

Since DSMZ 520 medium is optimal for growth of C. cellulovorans and DSMZ medium 135 Acetobacterium medium is optimal for the growth of C. aceticum, it was decided to test the medium with varying ratios to determine which ratio was best for the co-culture system. The following ratios were tested and compared (DSMZ 520:DSMZ 135): 1:1, 1:4, 2:3, 3:2, and 4:1. After preparation of the DSMZ mediums, they were separated into the corresponding ratio reaching a total volume of 45 mL. Each medium ratio had two different samples, one that was inoculated with C. *aceticum* and one that was inoculated with C. *cellulovorans*. This portion of the experiment allowed for monitoring of the growth of each bacterium in the medium ratios to determine an optimal ratio that suited both C. *cellulovorans* and C. *aceticum*.

Results

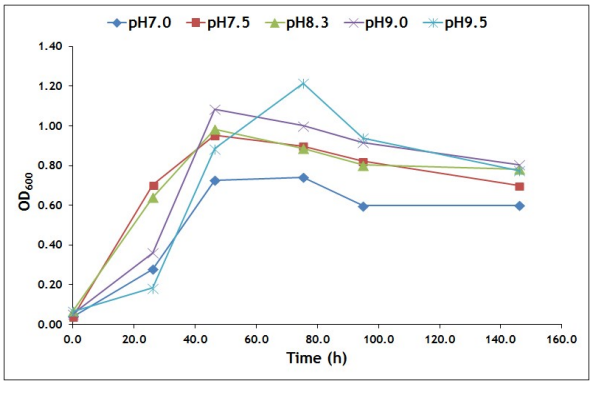

Figure 2. OD_{600} for *C. aceticum* under various pHs. Bacterial cell growth became abnormal as pH rose.

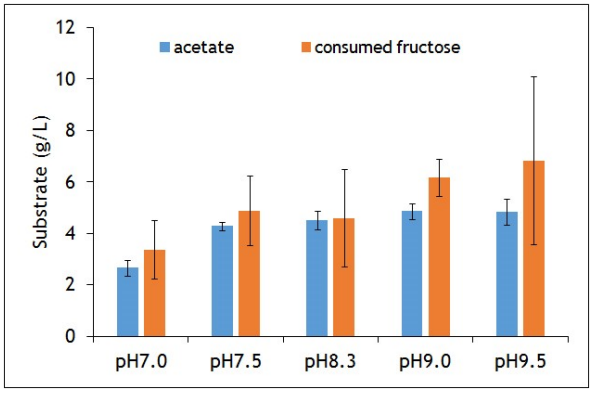

Figure 3. Ranges for substrate produced for *C. aceticum* under various pHs. The amount of fructose consumed rises as pH increases but the amount of acetate produced has insignificant variability from pH 7.5 onward.

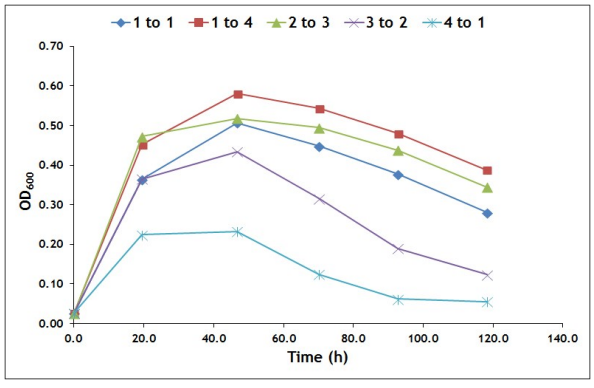

Figure 4. OD_{600} for *C. aceticum* with various ratios between DSMZ 520 medium for *C. cellulovorans* and DSMZ 135 Acetobacterium medium for *C. aceticum*. Bacterial cell growth varied from limited growth, as seen in the 4:1 ratio, to moderate growth, as seen in the 1:1 ratio.

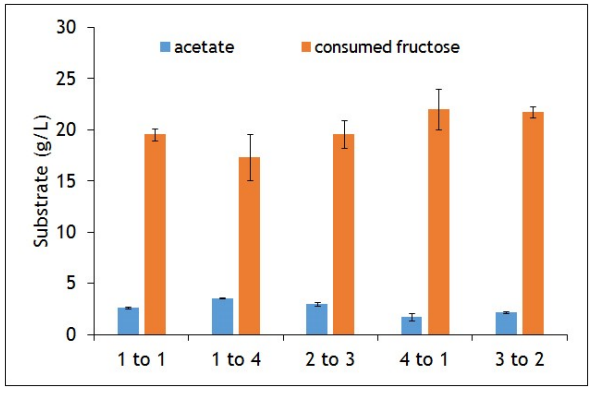

Figure 5. Ranges for substrate produced for *C. aceticum* with various ratios between DSMZ 520 medium for *C. cellulovorans* and DSMZ 135 Acetobacterium medium for *C. aceticum*. The amounts of fructose consumed and acetate produced have moderate variability over the ratios.

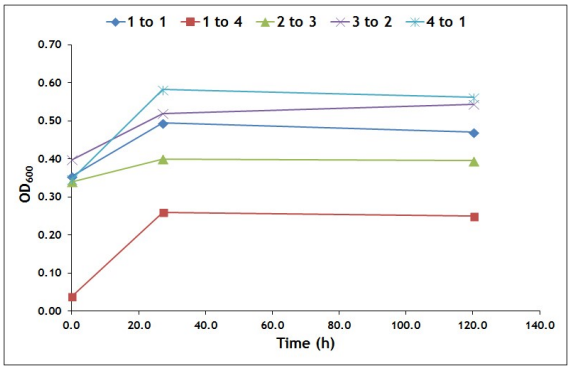

Figure 6. OD_{600} for *C. cellulovorans* with various ratios between DSMZ 520 medium for *C. cellulovorans* and DSMZ 135 Acetobacterium medium for *C. aceticum*. After the overnight culture, the OD_{600} values are similar. As evident by the graph, the various ratios do not affect the *C. cellulovorans* growth.

Discussion

4.1 Optimization of pH for C. cellulovorans and C. aceticum Co-culture

The concentrations of fructose consumed and acetate produced by *C. aceticum* at varying pHs were analyzed using high performance liquid chromatography and the results were recorded in Figure 3. The fructose consumed rose steadily with the pH of the samples while the product yield is consistent between pH 7.5 and 9.5. This further supports that a high final pH is not optimal for product yield. The data also suggests that increased fructose consumption does not increase acetate yield once a certain level of consumption is reached at about 4.89 g/L, observed at a pH of 7.5. The greatest ratio of acetate produced to fructose consumed, 4.287:4.890, is seen at a pH of 7.5. The production of acetate at a consistent level beyond pH 7.5 suggests that *C. aceticum* can survive at a higher pH than *C. cellulovorans*, but does not necessarily indicate that a higher pH is optimal. It can also be seen that at a pH of 7.5, *C. aceticum* displayed the greatest consistency in acetate yield between samples. Each acetate sample taken at a pH of 7.5 was within 0.33 g/L of the other samples in the group. As the pH of the groups rose, the range of the acetate yield in the samples increased as well, to as high as 1.011 g/L in the samples taken at a pH of 9.5. These observations combined with optimal cellular growth shown in Figure 2, suggest *C. aceticum* will perform optimally at a pH of 7.5.

Combining the previous knowledge that *C. cellulovorans* can survive between a pH of 7.0 and 7.5 and the obtained optimal pH of 7.5 for *C. aceticum,* an optimal range for the co-culture system was selected. The pH range of 7.0-7.5 was selected as optimal because it presented steady cellular growth without any abnormal jumps in bacterial concentration. This range was also selected because of the maximized ratio of the level of acetate produced to fructose consumed and its consistency in acetate yield.

4.2 Optimization of medium ratio for C. cellulovorans and C. aceticum Co-culture

Over the course of a five day period, the cellular density for each *C. aceticum* bottle was recorded. The optical densities for each ratio rose at varying rates over the course of the first 48 hours as depicted in Figure 4. After the 48 hour mark, the optical densities began to decline at varying rates based on which medium ratio formulation was used. Bacterial cell growth declined faster when less DSMZ 135 Acetobacterium medium was present. The 3:2 ratio and 4:1 ratio had the two lowest overall cellular density and declined at a more rapid speed. Due to these abnormalities, these two ratios were ruled out as being the optimal ratio for the medium formulation. The 1:1 ratio, 1:4 ratio, and 2:3 ratio all had a steady decline that mimicked typical cell death in media of a single type. In addition to a steady rise and decline, the 1:1 ratio stood out as having the most moderate growth out of the ratios. The 1:1 ratio fell in the middle of both the incline and decline, displaying a maximum OD_{600} of 0.51 at 46.7 hours.

As previously performed in the optimization of pH, the concentrations of fructose consumed and acetate produced were analyzed. Despite fluctuations in standard deviation with how much fructose was consumed, the standard deviation in terms of the amount of acetate produced varied minimally among the numerous trials as revealed in Figure 5. Looking at the ratio between acetate produced and fructose consumed, the 1:4 ratio produced the most acetate per fructose consumed at 0.2 g/L acetate produced per 1 g/L fructose consumed. This number can be compared to the favored 1:1 ratio, which produced 0.13 g/L acetate per 1 g/L fructose consumed. However, there was greater standard deviation with the amount of consumed fructose than any other ratio at 2.26 g/L. Comparatively, the 1:1 ratio had a standard deviation of 0.61 g/L. Weighing both qualifications equally--the standard deviation of the amount of fructose consumed and the ratio of acetate produced and fructose consumed--the 1:1 ratio boasts one of the lowest standard deviations in fructose consumed and the ratio of acetate produced and fructose consumed is significant enough to consider as an option. These observations coupled with the optimal cellular growth analysis in Figure 4 suggests that *C. aceticum* will perform optimally at a ratio of 1:1.

Despite the previous knowledge of how *C. cellulovorans* will perform at varying pHs, there was no knowledge of how *C. cellulovorans* would react when grown with the varying ratios of media. An inoculation was performed and the cellular density was examined once again at OD_{600}. The results were taken at the beginning, after a 24 hour period, and after an 118 hour period. The growth patterns were similar based on the shape of the curves. Conclusively, the various ratios do not affect *C. cellulovorans* growth.

After examining the results, an optimal ratio was selected. A ratio of 1:1 was selected due to moderate acetate yield to the amount of fructose consumed ratio. Furthermore, there was very little variability in the amount of acetate yield and consumed fructose. Finally, as exhibited by the optimal density results, the ratio of 1:1 had constant cell growth and a steady decline.

Conclusion

Two major medium optimizations for the co-culture between *C. aceticum* and *C. cellulovorans* have been found. A pH range of 7.0-7.5 for the medium has been characterized by the experiment as the optimal environment for both *C. aceticum* and *C. cellulovorans* cellular growth. In this selected pH range, the acetate yield to fructose consumed ratio was maximized. At the same time, the variability of acetate yield is minimal in the aforementioned pH range. More importantly, there were abnormal gaps of cell concentration for the other pH ranges. As a result, the steady cell growth follows a normal trend of bacterial cell concentration at this designated range. The appropriate ratio of the medium for *C. aceticum* growth was 1:1 (DSMZ 520: DSMZ 135). With this ratio, the acetate product yield along the fructose conversion ratio is most stable and the changeability of both acetate yield and consumed fructose is minimized. Last but not least, with the 1:1 ratio, there is the desired constant cell growth and steady decrease.

In the future, free-cell fermentation will be performed to see how the co-culture performs in a stirred tank bioreactor. The inoculation will be staggered as *C. aceticum* grows slower than *C. cellulovorans.* With three groups, the performance of the co-culture will be obvious. Group 1 will be the control group of *C. cellulovorans* for comparison, Group 2 will introduce the *C. cellulovorans* in the co-culture a day after the *C. aceticum* is inoculated, and Group 3 will introduce *C. cellulovorans* two days afterwards.

References

[1] Najafpour G, Younesi H (2006) Ethanol and acetate synthesis from waste gas using batch culture of *Clostridium ljungdahlii*. Enzy Microb Technol 38:223–228.

[2] Wang, Jufang, et al. "Engineering clostridia for butanol production from biorenewable resources: from cells to process integration." *ScienceDirect*, vol. 6, Nov. 2014, pp. 43-54. *ScienceDirect*, www.sciencedirect.com/science/article/pii/S2211339814000744. Accessed 16 Sept. 2016.

[3] Sim, J. H., Kamaruddin, A.H., Long, W.S., Najafpour, G., 2007. *Clostridium aceticum* – A potential organism in catalyzing carbon monoxide to acetic acid: Application of response surface methodology. Enzyme Microb. Technol. 40, 1234-1243.

[4] Tamaru, Y., Miyake, H., Kuroda, K., Nakanishi, A., Matsushima, C., Doi, R.H., Ueda, M., 2011. Comparison of the mesophilic cellulosome-producing *Clostridium cellulovorans* genome with other cellulosome-related clostridial genomes. Microb. Biotechnol. 4, 64–73. Tolonen, A.C., Haas, W., Chilaka, A.C., Aach, J., Gygi, S.P., Church, G.M., 2011. Proteome-wide systems analysis of a cellulosic biofuel-producing microbe. Mol. Syst. Biol. 7, 461.

Investigation of the intersection of cholesterol metabolism, neurodegeneration and lifespan in a C. elegans model of Parkinson's Disease

Samantha Glukhova, Siyuan Zhang, Guy A. Caldwell, Kim A. Caldwell

Faculty Mentor: Dr. Guy Caldwell

Department of Biological Sciences, The University of Alabama, Tuscaloosa, AL, 35487

Parkinson's disease (PD) is the second most common neurodegenerative disease affecting humans; due to the loss of dopaminergic neurons PD results in symptoms such as muscle tremors. Aging may represent a significant risk factor for the development of PD and an increase in PD occurrence is associated with increasing age. PD is characterized by the accumulation of α-synuclein (α-syn) protein aggregates in and around the neurons. We have developed an experimental model of PD in the roundworm Caenorhabditis elegans by expressing human α-syn in the dopaminergic neurons, to induce neuronal degeneration. This model is used to identify genetic components that act in conjunction with aging to contribute to PD. One such gene is daf-2, which, when mutated in C. elegans, extends lifespan and protects dopaminergic neurons from α-syn mediated cytotoxicity. A screen for genes involved with daf-2 identified nceh-1 as a potential functional modifier of genetic expression. Neutral cholesterol ester hydrolase (NCEH-1) the protein product of nceh-1, is a conserved enzyme that converts esterified cholesterol to free cholesterol. Although nceh-1 was identified by its relationship to the longevity gene daf-2, nceh-1 was found to have no impact on lifespan and the neuroprotection provided by nceh-1 is modulated by cholesterol.

Introduction

Aging is an important risk factor for many diseases, including Parkinson's disease (PD), as the decline of many physiological processes and the onset of a number of diseases are associated with increased age [6]. PD is characterized by the loss of dopaminergic neurons due to the accumulation of the α-synuclein (α-syn) protein that aggregates in and around the neurons [8]. The roundworm, *Caenorhabditis elegans* is a valuable model organism for identifying genetic regulatory mechanisms of aging and longevity [3]. In order to study PD, a *C. elegans* model expressing human α-syn in the animals' dopaminergic neurons it utilized; this causes age-dependent dopaminergic neurodegeneration. This model has been previously used to identify inherently neuroprotective genetic factors shared between worms and humans, which are either impacted by, or resistant to aging. Previous research identified *nceh-1* (Y43F8A.3) in a screen for genes that modulated aging and α-syn-induced dopamine neuron degeneration [4]. Considering the role of Neutral cholesterol ester hydrolase (NCEH-1) as an enzyme that converts esterified cholesterol to free cholesterol it is crucial to explore the role of cholesterol as an essential structural component for cellular membranes required for synapse formation [5]. Given the importance of cholesterol for neuronal health, the implications of NCEH -1 in cholesterol metabolism play a vital role in α-syn induced neurodegeneration in *C. elegans* model of PD.

To understand the role of cholesterol in neurodegeneration and overall health it is important to note that *C. elegans* is a cholesterol auxotroph, primarily using cholesterol as a precursor of reproductive signaling [11]. Neurons rely on the delivery of cholesterol in order to generate electrical impulses and maintain neuronal health. Thus, *C. elegans* possesses a remarkable advantage in the study of neurodegeneration related cholesterol metabolism as they lack the ability to biosynthesize cholesterol. This makes the function of NCEH-1 essential because it creates metabolically active free cholesterol from intracellular stored cholesterol esters. In this paper, NCEH-1 is studied for the first time as a neuroprotective modifier against α-syn-induced toxicity with its potential role in cholesterol metabolism.

Methods

C. elegans strains used in this work

Nematodes were maintained using standard laboratory procedures [1]. The *C. elegans* strains were provided by the Caenorhabditis Genetics Center, which is funded by NIH Office of Research Infrastructure Programs. The following strains UA44 (baIn11 [P_{dat-1}:: α-syn, P_{dat-1}::GFP]), UA196 (*sid-1(pk3321)*; baIn33 [P_{dat-1}::*sid-1*, P_{myo-2}::mCherry]; baIn11] and UA286 (baIn36 [P_{dat-1}::*sid-1*, P_{myo-2}::mCherry]; vtIs7[P_{dat-1}::GFP]) were generated as described previously [4].

RNA interference treatments

All bacteria for RNA interference (RNAi) were obtained from the Ahringer *C. elegans* library. Bacterial strains were isolated and grown overnight at 37°C in LB media containing 100 µg/ml ampicillin. NGM

plates containing 1mM IPTG were seeded with 250µl of RNAi culture and allowed to dry overnight. Six L4-stage worms were transferred onto corresponding RNAi plates to lay eggs overnight at 20°C. The offspring worms were continuously fed with the appropriate strain of RNAi bacteria and transferred to corresponding freshly plates as needed.

C. elegans neurodegeneration analysis

Worms were analyzed for Dopaminergic (DA) neurodegeneration as described previously [2]. Briefly, synchronized worms were grown at 20°C and scored using fluorescent microscopy techniques (Nikon Eclipse E800) for DA neuronal competency indicated by GFP at days 4, 6, 7 or 10 after hatching. Worms were considered normal when all six anterior DA neurons (four CEPs and two ADEs) were present without any visible signs of degeneration or morphological abnormalities. In total, at least three replicates of thirty adult worms were analyzed for each independent transgenic line or RNAi treatment. A Cool Snap CCD camera (Photometrics) driven by MetaMorph software (Molecular Devices) was used to acquire representative images. Statistics were analyzed using a one-way ANOVA or two-way ANOVA.

Results

Neutral Cholesterol Ester Hydrolase 1 Is Structurally and Functionally Conserved in C. elegans

In mammals, neutral cholesterol ester hydrolase 1 has been identified as the initial enzyme in reverse cholesterol transport and acts by converting cholesterol from its storage form, cholesterol ester, to its metabolically active form, free cholesterol. In *C. elegans*, NCEH-1 is the worm homolog of human neutral cholesterol ester hydrolase 1. It has 28% amino acid identity and 66% amino acid similarity with human NCEH-1. Most importantly the critical sites for hydrolase activity are conserved in the *C. elegans* NCEH-1 amino acid sequence [7]. These conserved critical sites allow a comparison to be made between the functions of the NCEH gene in *C. elegans* and its implications in humans in relation to Parkinson's disease.

To investigate whether cholesterol ester hydrolysis is functionally conserved in *C. elegans*, we quantified total body cholesterol levels of wild type (WT) N2 worms treated with empty vector (EV) control RNAi, *nceh-1* RNAi, and, as a negative control, *chup-1* (Cholesterol uptake associated) RNAi. When *nceh-1* was knocked down systemically in WT worms, total cholesterol increased compared to the EV control. This demonstrates that the conserved cholesterol ester hydrolysis activity of NCEH-1 is consistent with mammalian models in which deficient cholesterol ester hydrolase induces an accumulation of cholesterol ester and free cholesterol [12].

NCEH-1 is Protective against α-syn-Induced DA Neuron Neurodegeneration

We have previously reported that insufficient NCEH-1 activity enhanced α-syn aggregation in *C. elegans* body wall muscle cells [9]. Therefore, we wanted to extend the studies of α-syn toxicity and to explore how cholesterol would modulate the occurrence of α-syn aggregation in DA neurons. In *C. elegans*, overexpressing α-syn in DA neurons causes age and dose-dependent neurodegeneration. For example, as the worms age, there is a decrease in normal DA neurons. We see that at day 4, 69% of the population exhibited normal DA neurons, but at day 7, this number is reduced to 45%. Knocking down nceh-1 specifically in the DA neurons enhanced α-syn- induced neurotoxicity. When we analyzed the neurons at days 4 and 7, only 39% and 15% of worms displayed normal DA neurons, respectively. RNAi knockdown performed in DA neurons where α-syn was not expressed yielded no significant differences between nceh-1 depletion and EV knockdown. Thus, we can show that NCEH-1 is essential for DA neuron health during aging and enhanced DA degeneration by nceh-1 is α-syn dependent.

Exogenous Cholesterol Negatively Regulates α-Syn-Induced Neurodegeneration

Having established that knockdown of NCEH -1 increases cholesterol levels and enhances α-syn-induced neurodegeneration, we were next curious to explore the effects of exogenous cholesterol on α-syn neurotoxicity. As *C. elegans* do not naturally synthesize cholesterol, a cholesterol gradient was supplemented into the animals' growth medium. The α-syn animals were then raised on particular cholesterol concentrations and DA neurons were analyzed 7 days after hatching. Under normal cholesterol conditions (5µg/ml), 27% of worms displayed normal DA neurons, however, when the cholesterol level was reduced by 2.5 times (2 µg/ml), worms with normal DA neurons comprised 43% of the population. In contrast, exposure to high cholesterol (50 µg/ml) significantly enhanced DA neurodegeneration, as only 17% of the resulting worms displayed normal DA neurons (Figure 1). This data thus suggests that there exists a correlation between DA neurodegeneration and the amount of cholesterol exposure in α-syn expressing worms.

Depletion of Cholesterol Impairs the Neuroprotection of NCEH-1

As NCEH-1 prevents DA neurons from degenerating when cholesterol is decreased, we hypothesized that limiting cholesterol levels in NCEH-1 overexpression worms would result in neuroprotection. To

evaluate this, *C. elegans* larvae were exposed to growth medium either with or without cholesterol immediately upon hatching. We utilized a cholesterol gradient as described previously and observed that α-syn control worms displayed more intact DA neurons without cholesterol at days 5, 7, and 10 (Figure 2). However, when cholesterol was removed, NCEH-1 neuroprotection was significantly reduced. Specifically, at day 10, the percentage of NCEH-1 overexpression worms displaying normal DA neurons when cholesterol was removed from the medium was equivalent to α-syn control worms with normal cholesterol (Figure 2C). This data indicates that the neuroprotection provided by NCEH-1 is dependent on the presence of cholesterol.

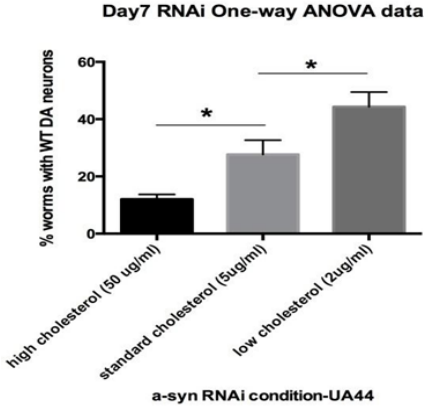

Figure 1: Percent of α-syn worms with WT DA neurons at day 7 when exposed to high, standard, and low cholesterol concentrations. Increasing cholesterol levels in the media resulted in enhanced DA neurodegeneration.

NCEH-1, as a Downstream Component in the IGF/ Insulin-Like Signaling Pathway, Has No Effect on C. elegans Lifespan

Previous studies found *nceh-1* functions in insulin signaling pathways. The gene *daf-2* was also determined in previous studies to function in insulin signaling pathways [10]. Importantly, when mutated in *C. elegans*, *daf-2* extends lifespan and protects dopamine neurons from α-syn aggregation and neurodegeneration. Because of the increase in the transcription levels of *nceh-1* in *daf-2* mutant worms compared to WT animals, we were interested in determining if the effects of NCEH-1 on longevity were similar and whether the role of NCEH-1in neuroprotection is related to lifespan.

It had been previously reported that the *daf-2* mutation inhibits α-syn aggregates in *C. elegans* body wall muscle cells and that knockdown of *daf-2* in DA neurons rescues α-syn toxicity induced neuronal death [9]. Since *nceh-1* transcription is up-regulated in the *daf-2* mutant background, it is possible that the neuroprotection observed in *daf-2* mutants is partially due to an increase of NCEH-1. A decrease in the loss of DA neurons was observed when *daf-2* was specifically knocked down in the DA neurons. When we double knocked down *nceh-1* and *daf-2*, the neuroprotective phenotype conferred by *daf-2* RNAi was reduced at the early stage and eliminated during aging by *nceh-1* deficiency.

DAF-16 is a FOXO transcription factor downstream of DAF-2 and its phosphorylation when *daf-2* is suppressed plays a critical role in the longevity by increasing the expression of anti-stress genes [10]. To explore the dependence of neuroprotection of NCEH-1 on DAF-16, we studied the knock down of both *daf-16* and *nceh-1* specifically in DA neurons of α-syn worms to determine whether the neuroprotection of NCEH-1 is dependent on the activation of DAF-16. The results exhibited a synergic effect on the enhancement of neurodegeneration by the double knockdown, implying that DAF-16 may not be the sole upstream regulator of the neuroprotective role of NCEH-1, and DAF-16 may act parallel to NCEH-1 in regard to α-syn-induced toxicity.

The mutant DAF-2 is associated with the mutation of *daf-2* which extends lifespan. Therefore, we asked if the neuroprotection associated NCEH-1 was due to reduced pathogenic development with extended lifespan and postponed chronological aging. The survival lifespan of worms was measured with and without RNAi systemic knockdown of *nceh-1* levels. The resulting survival data indicated that overexpressing NCEH-1 in DA neurons expressing α-syn did not significantly impact the aging process. Additionally, systemic knockdown of *nceh-1* did not alter the longevity resulting from *daf-2* mutation (Figure 3). Thus it can be inferred that the neuroprotection conferred by NCEH-1 is not due to an extension of lifespan.

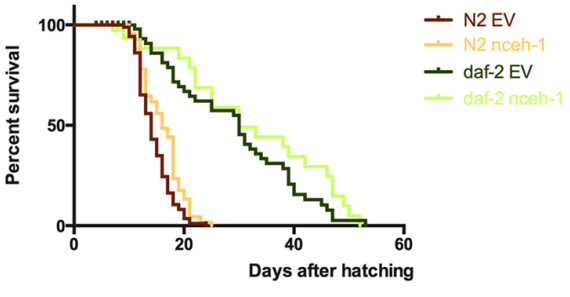

Figure 3: Lifespan of N2 and *daf-2* mutant worms on both EV and *nceh-1* RNAi conditions and the percent of worms that survived days after hatching

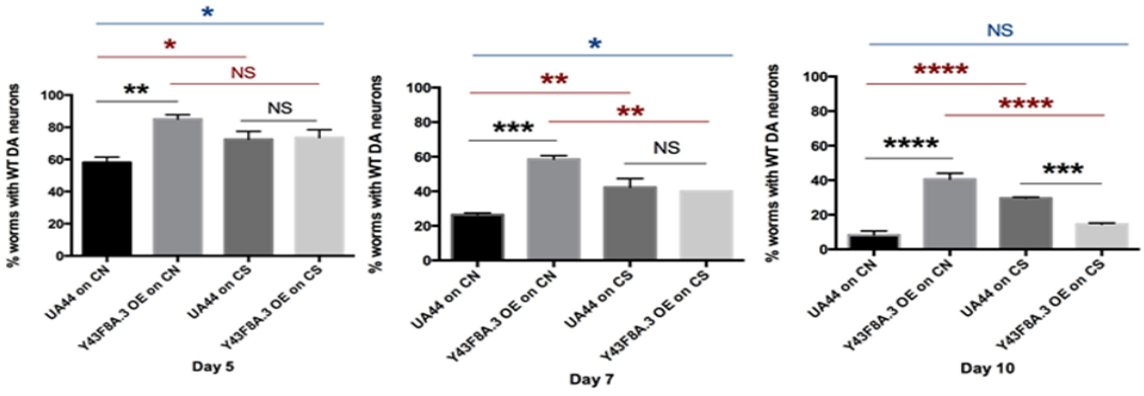

Figure 2: (A, B, C): Percent of UA44 (α-syn) and Y43F8A.3 OE (NCEH-1 overexpressed) worms with WT DA neurons at day 5,7,10 when exposed to standard cholesterol concentrations (cholesterol normal) or reduced cholesterol (cholesterol starvation). Reducing cholesterol levels in the media protects DA neurons, but also reduces the protection provided by nceh-1. CN: Cholesterol Normal plates; CS: Cholesterol Starvation plates Analysis (n=30/trial in triplicate) ; * $p<0.05$; ** $p<0.005$; *** $p<0.0005$; One-way ANOVA

Discussion

The aforementioned data indicated the conserved hydrolysis activity of NCEH-1 accounts for its protection against α-syn-induced neurodegeneration. The mechanism for NCEH-1 neuroprotection against α-syn toxicity was investigated based on its regulation of cholesterol metabolism. Deficient NCEH-1 activity resulted in an accumulation of cellular cholesterol, which was shown to be harmful to neuronal health with α-syn. The presence of cholesterol is essential to the neuroprotection of NCEH-1, and decreased levels of cholesterol are correlated with diminished neuroprotection provided by NCEH-1. Collectively, we have discovered the neuroprotective role of NCEH-1 and clarified the relationship between NCEH-1-influenced cholesterol metabolism and α-syn toxicity in the neurodegeneration and lifespan of *C. elegans.*

References

[1] Brenner, S. *et al*. (1974). The Genetics of Caenorhabditis elegans. Methods 77, 71–94. doi:10.1111/j.1749-6632.1999.tb07894.x

[2] Cao, S. *et al*. (2005). Torsin-mediated protection from cellular stress in the dopaminergic neurons of Caenorhabditis elegans. J. Neurosci. 25, 3801–3812

[3] Conti B. *et al.* (2008) Considerations on temperature, longevity and aging. Cell Mol Life Sci CMLS 65:1626–1630.

[4] Cooper A. *et al.* 2006. Alpha-synuclein blocks ER-Golgi traffic and Rab1 rescues neuron loss in Parkinson's models. Science (80). 313, 324–328

[5] De Chaves. *et al.* (1997) Role of Lipoproteins in the Delivery of Lipids to Axons during Axonal Regeneration. The Journal of Biological Chemistry, 272, 30766-30773.

[6] Hahm J. *et al.* (2015) *C. elegans* maximum velocity correlates with healthspan and is maintained in worms with an insulin receptor mutation. Nature.

[7] Igarashi M. *et al*. (2010). Targeting of neutral cholesterol ester hydrolase to the endoplasmic reticulum via its N-terminal sequence. J. Lipid Res. 51, 274–285.

[8] Kenyon C. *et al.* (1993) *C. elegans* mutant that lives twice as long as wild type. Nature 366, 461–464

[9] Knight A. *et al*. (2014) The Glycolytic Enzyme, GPI, Is a Functionally Conserved Modifier of Dopaminergic Neurodegeneration in Parkinson's Models. Cell Metabolism 20(1):145-57.

[10] Murphy C.T. *et al*. (2003). Genes that act downstream of DAF-16 to influence the lifespan of Caenorhabditis elegans. Nature 424, 277–283

[11] Rauthan M. *et al*. (2011). The mevalonate pathway in C. elegans. Lipids Health Dis. 10, 243.

[12] Sekiya M. *et al*. (2009). Ablation of Neutral Cholesterol Ester Hydrolase 1 Accelerates Atherosclerosis. Cell Metab. 10, 219–228.

A Review of the Molecular Basis for Nicotine Addiction

Brian Smithers

Faculty Mentor: Dr. Guy Caldwell
Department of Biology, The University of Alabama, Tuscaloosa, AL 35487

Nicotine addiction is a dependence on the drug nicotine, a compound found in tobacco. Tobacco can be smoked, absorbed through the mucous membranes of the mouth, or insufflated to provide the stimulant effects associated with nicotine. Nicotine acts on nicotinic acetylcholine receptors (nAChRs) located at neuronal junctions within the central and peripheral nervous system and at neuromuscular junctions throughout the body. Nicotine stimulates the opening of the ligand-gated ion channel, allowing depolarization of the post-synaptic region and causing muscle contraction. Nicotine is addictive mainly due to the release of dopamine through the mesolimbic "reward" pathway. However, tobacco also contains monoamine oxidase inhibitors, which prevent the breakdown of the dopamine that is released and have been shown to increase the addictiveness of nicotine. Most nicotine cessation treatments currently available are a form of nicotine replacement therapy, which involves using a nicotine-containing product like a transdermal nicotine patch or chewing nicotine gum, and some nicotinic acetylcholine receptor (nAChR) partial agonists, such as varenicline, reduce nicotine withdrawal symptoms to aid in the cessation process. Certain antidepressants, like buproprion, are also often prescribed to help those who wish to stop smoking.

Introduction

Nicotine is a highly addictive drug that functions as a stimulant. Despite the well-known harmful effects of smoking and widespread smoking prevention campaigns, many people still regularly smoke cigarettes or use other forms of tobacco [4]. Smoking is the leading preventable cause of death, resulting in upwards of 480,000 smoking-related deaths in America each year [16]. This has increased from the average per year of 438,000 reported by the CDC [4]. In, nicotine causes a conformational change that allows ions to flow through the newly opened channel. The result is an excitatory post-synaptic potential in neurons and muscle contraction when a muscle is post-synaptic to the nAChR. Monoamine oxidase (MAO) is an enzyme that oxidizes monoamines in the brain – these include serotonin, norepinephrine, and dopamine, among others. MAOs are the target of a class of compounds known as monoamine oxidase inhibitors (MAOIs). The inability to break down these monoamines allows for increased effectiveness of the monoamines already present, leading to an antidepressant effect and/or increased strength and duration of feelings of pleasure. Tobacco, the source of most nicotine, contains naturally-occurring MAOIs that reinforce the feeling of pleasure associated with using nicotine and potentially increase the addictive qualities of the drug. The purpose of this review is to examine the relationship of nicotine dependence to the dopamine release caused by nicotine, and to relate the effect of the MAOIs found in tobacco to an increase in addictiveness of nicotine. Finally, this review will examine current nicotine cessation therapies.

Acetylcholine Receptors - Structure and Function

There exist two classes of acetylcholine receptors, each named after the ligand for which it has higher affinity. Muscarinic acetylcholine receptors (mAChRs) have a higher affinity for muscarine than for nicotine, and nAChRs have higher affinity for nicotine. mAChRs are G-protein- coupled receptors which can regulate cardiac activity, among other things. Only nAChRs will be examined in detail, as mAChRs are outside the scope of this review.

nAChRs are ion channels found in both the central and peripheral nervous system. They are composed of five subunits, which can be a combination of five alpha subunits or a mixture of alpha and beta subunits. The most common subtypes in the brain are the $\alpha4\beta2$ and $\alpha7$ subtypes. $\beta2$ subunits have the highest affinity for nicotine and other nAChR agonists [18].

When a ligand binds to a nAChR, it induces a conformational change involving the rotation of the α-helices. This rotation causes the barrel-like α-helices to move farther apart, resulting in a channel through which ions – here sodium, calcium, and potassium – may flow[6]. Cells harness this ion gradient for various functions dependent upon location. nAChRs may be found at the neuromuscular junction or at a neuronal junction. At the neuromuscular junction, this ion flow causes muscle contraction; at a neuronal junction, it results in depolarization and signal transduction from the pre- to post-synaptic neuron. These are the same effects caused by acetylcholine binding as the ligand instead of nicotine. Nicotine simulates a larger concentration of acetylcholine, and has higher affinity for the receptors. This explains much of the stimulating effect of nicotine.

Acetylcholine Receptors – Desensitization

Desensitization is a process by which receptors are regulated. It occurs in one of two ways – either the receptor can be removed from its native membrane and broken down, or the receptor can undergo a conformational change into an inactive state. Acetylcholine receptors mainly undergo the latter, known as acute desensitization, so not many receptors are lost. Interestingly, despite having a conformation that is not conducive to the ion transport function of a normal nAChR, the desensitized nAChRs have a higher affinity for the appropriate ligands, including nicotine [15]. This is due to a greater ability for ligands to bind to the binding sites in the protein when in its inactive conformation. [18, 15]. While the exact mechanism for desensitization of nAChRs is not yet known, Ochoa et al (1989) explains that the mechanism must work primarily through phosphorylation with the action of a series of protein kinases [15].

Another interesting aspect of nAChR desensitization is the importance of the balance of active and desensitized receptors and their role in the physiological response to nicotine. It stands to reason that the α subunit must be able to desensitize the receptor by itself, as there are homomeric α7 nAChRs. An effort to determine the purpose and mechanism of desensitization was made by examining mutations in various components of the mechanism [19]. These mutations can cause a form of epilepsy in humans, and other excitotoxic effects are also observable. It seems that desensitization of nAChRs serves in part to limit excessive stimulation [19, 15].

Physiological Response to Nicotine

Nicotine has a range of effects on the body. Initial uptake of nicotine causes a release of epinephrine, which is associated with a range of effects such as increased heart rate and blood pressure [8]. Male and female smokers have an average resting heart rate 6.5 and 6.4 beats per minute higher, respectively, than non-smokers within the same age range [17]. In addition, the heart rate of smokers increases more slowly during exercise, and does not reach the estimated maximum for the specified age range[17]. Nicotine also causes increased cognition. Rezvani and Levin (2001) found that rats exposed to an acute dose of nicotine displayed increased memory and avoidance behavior [20]. Rats given chronic nicotine exposure displayed largely the same cognitive benefits, but a higher dose was required to maintain the effects after a few days due to increased tolerance [20].

While many of the effects of nicotine are due to the activation of ion channels within nAChRs, some effects have been linked to the desensitized receptors. Nicotine from one cigarette can rapidly (within 1 minute of inhalation) bind to 88% of α4β2 nAChRs in the brain, which leads to desensitization of up to 50% of α4β2 receptors [2, 18]. Chronic nicotine exposure results in nearly all nAChRs existing in the desensitized state, with a saturated base level of nicotine. This desensitization has an antidepressant effect, which has been shown in both human and animal models [18].

The Role of Dopamine in Nicotine Addiction

Dopamine plays a role in dependence on various addicting drugs, including nicotine, cocaine, and amphetamine. The mesolimbic pathway is known as the reward pathway in the brain. It is the pathway between the ventral tegmental area (VTA), an area with a high concentration of dopamine and serotonin neurons, and the limbic system and prefrontal cortex. Stimulation of the ventral tegmental area causes a release of dopamine, which can serve to reinforce behavior and exacerbate addictive qualities of drugs. Further, the mesolimbic pathway is responsible for much of the pleasurable feeling due to nicotine use. nAChRs located on dopamine neurons in the VTA respond to nicotine by releasing a dose-dependent amount of dopamine [5]. The majority of this dopamine is released to the nucleus accumbens, another region of the brain associated with reward and motivation [7].

As mentioned previously, dopamine release is not characteristic of nicotine alone. Ethanol is another drug that can cause a release of dopamine to the mesolimbic system. When used in conjunction with nicotine, there occurs a synergistic effect by which the pleasure response from each drug increases the total response more than the sum of its parts [22]. This may explain the phenomenon known as the 'drunk cigarette,' where non-smokers choose to smoke cigarettes while under the influence of alcohol [22].

Dopamine is a monoamine that is oxidized by monoamine oxidase. Monoamine oxidase inhibitors limit the function of this enzyme, resulting in lower breakdown of dopamine and other monoamine neurotransmitters. As mentioned previously, this increases the effects of the dopamine. This has a compounding effect with nicotine, as the flood of dopa-

mine caused by nicotine is not broken down as it normally would be. This leads to further behavioral reinforcement of the reward-causing behavior – in this case, nicotine use.

Unfortunately, this does not just affect those taking MAOIs as antidepressants. Tobacco contains naturally-occurring monoamine oxidase inhibitors; the primary MAOIs found in cigarette smoke are harman and norharman alkaloids [9]. Smokers have, on average, lower activity of MAO-A and MAO-B – two isozymes of monoamine oxidase - in the brain than non-smokers [9].

The release of dopamine is not only caused by smoking; it can also be released with environmental stimuli, leading to the desire to smoke [11]. When exposed to certain stimuli, such as a blinking light or being moved to a specific location, rats have been shown to increase self-administration of nicotine [11, 3, 14]. In humans, this translates into a craving to smoke at a certain time of day, while in a certain mood, or while in a certain familiar location.

Smoking and Mental Illness

Many other factors have been correlated with nicotine addiction. Chief among them is mental illness.Smoking and mental illness are irrefutably intertwined. Lasser et al examined the National Comorbidity Survey and found that, for both current and lifetime smokers, a person with mental illness was 2.7x as likely to be a smoker than somebody without mental illness [13]. This is likely due to the nAChR desensitization explained above – people with mental illness may self-medicate with nicotine due to the antidepressant effects. Despite this, or perhaps because of this, smokers with a mental illness have a higher quit rate than smokers without a mental illness.

These antidepressant effects are not shown only by nicotine. nAChR antagonists, such as dextromethorphan, inhibit the action of nAChRs, producing a similar functional effect to desensitization, and some antidepressant medications act as NAChR antagonists. For example, many common tricyclic antidepressants have been shown to inhibit nAChRs, potentially explaining, at least in part, their effectiveness [21].

Current Treatments for Nicotine Addiction

Nicotine addiction remains extremely common despite the widespread availability of smoking cessation products, both prescribed and over-the- counter. One main therapy for smoking cessation is the use of nicotine replacement therapy. Nicotine replacement therapy involves the use of nicotine-containing products, such as nicotine gum and/or the nicotine patch, to replace the nicotine that was originally gained through smoking. The goal of nicotine replacement therapy is to slowly reduce the amount of nicotine being consumed, eventually tapering off completely. Hsia, Meyers, and Chen (2016) performed a meta-analysis and determined that nicotine replacement therapy works best when multiple types of replacement therapy are combined into a tapering schedule [10]. For example, a patient might use the highest dose nicotine patch in combination with several pieces of nicotine gum per day as needed to fight the urge to smoke. After a few weeks, this patient would lower the dose of the nicotine patch and continue using the gum in lesser amounts per day. Eventually, following this pattern, the patient would successfully cease using nicotine in any form and have a lower chance to begin smoking again.

Another increasingly common smoking cessation treatment is varenicline (Chantix™). Varenicline is an α4β2 partial agonist [12]. The drug binds to the nAChR receptors and limits the positive effects of nicotine use. In addition, varenicline binding to nAChRs lessens some of the withdrawal symptoms of smoking cessation [12].

A final smoking cessation treatment is buproprion, a prescription antidepressant. Buproprion is often prescribed to aid in smoking cessation; however, some data suggests it is no more effective than over-the-counter nicotine replacement therapy [12, 1]. This antidepressant likely has the same nAChR inhibitory qualities of certain other antidepressants, and simulates a desensitized state for most nAChRs in the brain.

Of the treatments listed, the partial agonist varenicline is most effective as a smoking cessation device. However, varenicline still only has an effective cessation rate of 22-23% [12, 1].

Conclusion

Nicotine is extremely addictive due to a combination of neuronal responses to nicotine exposure and the presence of MAOIs in tobacco that increase the behavioral reinforcement of dopamine in the mesolimbic pathway. Despite the well-known risks of tobacco smoke, millions of individuals continue to smoke. This can be attributed, in part, to the lack of effective smoking cessation treatment; although many over-the-counter and prescription treatments are available, these treatments are not particularly effective Current research indicates that drugs like varenicline, a partial

agonist of nAChRs, are the most effective treatment currently on the market. Future research should explore other partial agonists of the nAChRs to determine if a more effective smoking cessation drug can be developed.

Works Cited

[1] Athanasakis K, Igoumenidis M, Karampli E, Vitsou E, & Kyriopoulos J. (2011). PRS33 A Cost effective analysis of Varenicline versus bupropion and nicotine replacement therapy in Greece. Value in Health, 14: A493.

[2] Brody AL et al. (2006). Cigarette smoking saturates brain α4β2 nicotinic acetylcholine receptors. Archives of General Psychiatry, 63: 907-915.

[3] Caqqiula et al. (2002). Environmental stimuli promote the acquisition of nicotine self- administration in rats. Psychopharmacology, 163: 230-237.

[4] CDC. (2005). Annual smoking-attributable mortality, years of potential life lost, and productivity losses: United States, 1997-2001. Morbidity and Mortality Weekly Report, 54: 625-628.

[5] Chen Y, Sharples TJ, Phillips KG, Benedetti G, Broad LM, Zwart R, Sher E. (2003). The nicotinic α4β2 receptor selective agonist, TC-2559, increases dopamine neuronal activity in the ventral tegmental area of rat midbrain slices. Neuropharmacology, 45: 334-344.

[6] Doyle DA. (2004). Structural changes during ion channel gating. Trends in Neurosciences, 27: 298-302.

[7] Fung YK & Lao YS. (1992). Chronic effects of nicotine on mesolimbic dopaminergic system in rats. Pharmacology Biochemistry and Behavior, 42: 57-63.

[8] Gajewska M, Worth A, Urani C, Briesen H, & Schramm KW. (2014). The acute effects of daily nicotine intake on heart rate – A toxicokinetic and toxicodynamic modelling study. Regulatory Toxicology and Pharmacology, 70: 312-324.

[9] Herraiz T, Chapparo C. (2005). Human monoamine oxidase is inhibited by tobacco smoke: β- carboline alkaloids act as potent and reversible inhibitors. Biochemical and Biophysical Research Communications, 326: 378-386.

[10] Hsia SL, Myers MG, & Chen TC. (2016). Combination Nicotine Replacement Therapy: Strategies for Initiation and Tapering. Preventative Medicine, 97: 45 -49.

[11] Itasaka M, Hanasawa M, Hironaka N, Miyata H, & Nakayama K. (2012). Facilitation of Intracranial Self-Stimulation Behavior in Rats by Environmental Stimuli Associated with Nicotine. Physiology and Behavior, 107: 277-282.

[12] Jorenby DE, Hays JT, & Rigotti NA et al. (2006). Efficacy of Varenicline, an α4β2 Nicotinic Acetylcholine Receptor Partial Agonist, vs Placebo or Sustained -Release Bupropion for Smoking Cessation. Journal of the American Medical Association, 296: 56-63.

[13] Lasser K, Boyd JW, Woolhandler S. (2000). Smoking and Mental Illness: A population-based prevalence study. Journal of the American Medical Association, 284: 2606-2610.

[14] Neugebauer NM, Cortright JJ, Sampedro GR, & Vezina P. (2014). Exposure to nicotine enhances its subsequent self-administration: Contribution of nicotine-associated external stimuli.

[15] Ochoa et al. (1989). Desensitization of the nicotinic acetylcholine receptor: Molecular mechanism and the effect of modulators. Cellular and Molecular Neurobiology, 9: 142-166.

[16] Office of the United States Surgeon General. (2014). 50 Years of Progress: A Report of the Surgeon General, 2014.

[17] Papathanasiou et al. (2012). Effect of smoking on heart rate at rest and during exercise, and on heart rate recovery, in young adults. Hellenic Journal of Cardiology, 54: 168-177.

[18] Picciotto MR, Addy NA, Minneur YS, & Brunze; Brunzell DH. (2007). It's not "either/or": activation and desensitization of nicotinic acetylcholine receptors both contribute to behaviors related to nicotine addiction and mood. Progress in Neurobiology, 84: 329-342.

[19] Quick MW & Lester R. (2002). Desensitization of Neuronal Nicotinic Receptors. Developmental Neurobiology, 53: 457-478.

[20] Rezvani AH & Levin ED. (2001). Cognitive effects of nicotine. Biological Psychiatry, 49: 258-267.

[21] Shytle et al. (2002). Nicotinic Acetylcholine Receptors as targets for antidepressants. Molecular Psychiatry, 7: 525-535.

[22] Soderpalm B, Ericson M, Olausson P, Blomqvist O, & Engel JA. (2000). Nicotinic Mechanisms Involved in the Dopamine Activating and Reinforcing

Properties of Ethanol. Behavioural Brain Research, 113: 85-96.

Isolation and Characterization of a *Staphylococcus epidermidis* bacteriophage

Madeleine Hull [1] , Steven Scaglione[1]

[1]*Department of Biological Sciences, The University of Alabama, Tuscaloosa, Alabama 35487*

The discovery of virulent phage and their cultivation has led many researchers to look for new ways to utilize their bactericidal qualities in a therapeutic context. Up to this point, few phage species have been characterized to attack Staphylococcus epidermidis, a CoNS staphylococci that is a common cause of nosocomial infections. In an age of declining antibiotic efficacy and fewer new antibiotics being produced, it is necessary for researchers search for new ways, such as phage therapy, to treat bacterial infections. Increasing numbers of phage have been found to attack and lyse bacterial pathogens, yet few phage that attack S. epidermidis RP62a have been discovered. In this experiment, we employed investigatory methods to extract phage from raw sewage, co-culture the lysate with pathogenic bacteria, purify the lysate, and generate a high titer for visual characterization. Through these methods, we were able to produce a high-titer lysate that shows stability in refrigerated storage conditions and can be imaged via transmission electron microscopy. After imaging the phage and observing its morphology, we have determined it belongs to the family Myoviridae. We also subjected our phage, Mysterymachine, to genotypic and phenotypic testing by utilizing nuclease and restriction enzyme digestion, host range analysis, and growth dynamics. Our phage is effective against S. epidermidis ATCC12228 and S. epidermidis RP62a at an MOI=1 and forms plaques on 4 different strains of S. epidermidis.

Introduction

Staphylococcus epidermidis is a Gram-positive and coagulase-negative staphylococcus (CoNS) species that is part of the native flora of healthy human beings (1-3). The species is generally located on human skin and mucosal membranes [1-3], and includes many opportunistic pathogens that are often associated with medical devices and implants. *S. epidermidis* is a prevalent cause of nosocomial infections, where it can form biofilms that serve as infectious reservoirs that can be very dangerous for a patient [1-4]. These biofilms are more resistant to antibiotics and immune system components compared to planktonic bacteria, and are becoming a larger concern in the modern age [5]. Therefore, it is necessary to research novel methods for treating and preventing *S. epidermidis* biofilm infections.

The use of bacteriophage to treat bacterial infections, also known as phage therapy, has gained attention in recent years, especially as resistance to antibiotics becomes more widespread [6-8]. Many advantages come with using phage over antibiotics, such as their bactericidal effects (destroying the viability of a bacterium], little impact on the human microbiome, and their unlikelihood to contribute to bacterial resistance [9]. Additionally, virulent phages can be used to treat bacterial infections without harming humans or animals [8]. However, a phage must be well characterized before deciding if it is a good candidate for phage therapy. For example, the use of temperate phage is not ideal for phage therapy because they can transfer virulence factors to bacteria. Additionally, temperate phage can potentially inhabit a bacterium as a prophage instead of lysing the cell and combating the bacterial infection directly [9,10]. Little is known about phages that attack *S. epidermidis,* and none show strictly virulent behavior, so investigative methods must be employed to discover novel virulent phage for treatment of *S. epidermidis* infections with phage therapy [10].

The importance of isolating and characterizing a novel phage for use in treatment of *S. epidermidis* infections is clear. In this work, a phage was isolated from raw sewage found at a local wastewater treatment plant. The phage is effective against *S. epidermidis* RP62a and *S. epidermidis* ATCC12228 at a multiplicity of infection (MOI) of 1 and exhibits plaque formation on *S. epidermidis* LM1680 and *S. epidermidis* 1457. Mysterymachine is presumed to be virulent by plaque analysis, and is stable in a long-term, refrigerated setting, potentially making it a good candidate for phage therapy. Additionally, after visualization under transmission electron microscopy, we determine the structure of the phage to be that of a *Myophage*.

Materials and Methods

Sterile Media Preparation

20 g of tryptic soy agar and 500 mL of dH_2O were combined in a 1 L bottle containing a stir bar and autoclaved to make sterile TSA agar for plating. 6 g of tryptic soy broth and 200 mL of dH_2O were combined twice and autoclaved to make two aliquots of sterile TSB. This process was repeated as agar or TSB was needed. To make sterile 0.5x Heart Infusion Agar (HIA), 4 g of HIA was combined with 200 mL of dH_2O and autoclaved. To make sterile "Sloppy Top Agar," 1.3 g of HIA was combined with 100 mL of dH_2O and autoclaved.

Collection of Wastewater

Approximately 200 mL of raw sewage was collected from Hillard Fletcher Wastewater Treatment Plant (4010 Kauloosa Ave., Tuscaloosa, AL 35401) using a sterile ~250 mL collection bottle. The sample was placed in a zip-top bag containing absorbent material and placed in a cooler with approved EHS biohazard signage.

Phage Enrichment

30 mL of raw sewage was placed into a 50 mL conical tube and centrifuged for 10 min at 4ºC. During the spin, 20 mL of sterile TSB, 40 µL of $CaCl_2$, and 1 mL of host organism (*Staphylococcus pseudointermedius* ED99) were combined into a sterile 250 mL flask. Following the spin, 20 mL of the phage source was added to the flask. Flask was incubated overnight at 160 rpm at 37ºC.

Phage Extraction and Co-culture

Overnight co-culture was poured into a labeled 50 mL conical and centrifuged at 10,000xg for 5 min at 4ºC.Two 0.45 µm syringe filters were attached to two 10 mL syringe barrels. Each student poured ~10 mL of supernatant into a syringe and filtered it into a 15 mL conical. (Remaining pellet in 50 mL conical was discarded into the biohazard bin.) In a sterile 250 mL flask, 20 mL of fresh TSB, 40 µL of $CaCl_2$ (while swirling), 20 mL of filtered lysate, and 1 mL of *S. pseudointermedius* ED99 were combined. The flask was incubated overnight at 160 rpm at 37ºC. (All tubes and flasks were labeled with initials, pathogen, phage source, and date.)

Plaque Detection using Agar Overlay Method

Two TSA+ 5mM $CaCl_2$ plates were labeled "Experimental" and "NC" and pre-warmed at 37ºC for ~10 min. Two 15mL conical tubes were also labeled "NC" and "Experimental." In each conical, 4 mL of HIA molten top agar, 4 µL of $CaCl_2$, 100 µL phage lysate (or 100 µL TSB for NC), and 100 µL overnight host culture were combined; conical was immediately inverted gently 3 times and poured evenly onto the pre-warmed plates. Plates were tilted to allow agar to cover plate completely and left to sit undisturbed for ~10 min (or until dry.) Plates were then incubated upside-down at 37ºC overnight. Supernatant was stored at 4ºC with Parafilm around lid.

Plaque Assay using Enriched Phage Lysate

Three TSB+$CaCl_2$ plates were labeled (NC, 0, 1, 2 with host organism, phage sources, initials, and date) and pre-warmed at 37ºC for ~10 min. A separate plate was labeled as shown below. A dilution scheme was made with a phage lysate by putting 90 µL of TSB into 1.5 mL tubes labeled "1", "2", and "3". 10 µL of the "low titer" lysate was placed into the tube labeled "1" and gently mixed to make the 1:10 dilution. This method was repeated for tubes "2" and "3" to make 1:100 and 1:1000 dilutions. Next, 4 mL HIA top agar, 4 µL $CaCl_2$, and 100 µL of TSB or lysate, and 100 µL overnight host culture were combined into 15 mL conical tubes. These tubes were inverted 3 times and poured onto their respective TSA plates (labeled NC, 0, 1, 2). The plates were allowed to sit for ~10 minutes. Within a separate conical tube, 4 mL HIA top agar, 4 µL $CaCl_2$, and 100 µL of host organism were combined. The tube was inverted gently three times, poured on the separate plate, and allowed to solidify for ~10 minutes. On the plate labeled as above, 10 µL drops of undiluted lysate and the 1:10, 1:100, 1:1000 dilutions were placed on top of the numbers written on the plate, and the plate was tilted 45°C to allow the drops to travel down the plate. Drops were allowed to dry, and plates were incubated upside-down overnight at 37°C.

Phage Lysate Purification

Four TSA+$CaCl_2$ plates were warmed for ~10 minutes at 37°C and labeled all of them with initials, phage source, host organism, and date, and each individual plate with "NC", "0", "1", and "2". A plaque was chosen off a plate from the previous plaque experiment and excised with a 1000 µL pipette tip and expelled into a 1.5 mL tube containing 1 mL of TSB. The 1.5 mL tube was vortexed to release phage into the TSB. The suspension was then centrifuged for 2 minutes at 12,000 rpm to produce a "low titer lysate". 1:10 and 1:100 dilutions were made using techniques referenced previously, and were labeled "1" and "2". Four 1.5 mL were labeled "NC", "0", "1", and "2", and 100 µL of overnight *S. epidermidis* RP62a, 4 µL of 5 mM $CaCl_2$, 10 µL of TSB, undiluted lysate, 1:10, or 1:100 (respectively) were placed in each tube. The tubes were then placed in a 4°C cold room for 10 minutes. In four 15 mL conical tubes, 4 mL of HIA molten top agar and the entire contents

(~114 µL) of each 1.5 mL tube (phage-host mixture) were combined and inverted 3 times gently. Each mixture was poured on their respective TSA plate, allowed to coat the plate evenly, and left to solidify for ~10 min. The plates were then turned upside down and placed in an incubator overnight at 37°C.

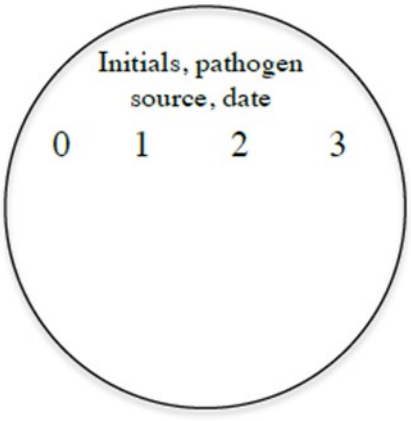

Preparing High Titer Phage Lysate with Sloppy Agar

Three TSA+ 5mM $CaCl_2$ plates were labeled "NC", "+", and "+", and pre-warmed at 37°C for ~10 min. A plaque was then picked from a previous phage isolation plate and expelled into 500 mL of sterile TSB inside a 1.5 mL microtube. The tube was capped securely, vortexed for 10 seconds to release phage, and centrifuged for 2 min at 12,000 rpm to generate final low titer lysate. During the spin, one of three 1.5 mL microtubes was labeled "NC" and the other two were labeled with a "+". The following were combined in order inside each microtube: 300 overnight *S. epidermidis* RP62a culture, 7 µL of 5 mM $CaCl_2$, and 200 µL of either sterile TSB ("NC") or undiluted low-titer lysate ("+"). The tubes were then placed in a 4°C cold room for 10 minutes. After the mixtures cooled, three 15 mL conical tubes were labeled "NC", "+", and "+". Into each tube, 7 mL of HIA Sloppy Agar and the entire contents of the 1.5 mL tubes (corresponding with the labeling on the tubes) were combined and inverted 3 times. This mixture was then poured on top of respectively labeled plates and allowed to sit undisturbed on the bench for ~10 min. The plates were then placed upright in the incubator and left overnight at 37°C. Following the incubation period, plates with plaques were used to prepare the high-titer lysate. A sterile scraper was used to scrape the sloppy agar off the plate (making sure that none of the bottom agar gets into the mixture) and into a 50 mL conical tube. This was repeated for both plates labeled "+". A serological pipettor was used to place 25 mL of TSB into each of the 50 mL tubes containing sloppy agar. The tubes were capped securely and vortexed for 5 minutes to release the phage. The mixtures were then centrifuged at 8,000 rpm for 5 minutes and filtered using a single filter bottle assembly.

Titer Assessment

Using the methods outlined in "Plaque Detection using Agar Overlay Method" (edit: no phage was added to mixture prior to pouring), the phage titer was assessed by placing drops of different phage dilutions onto a grid drawn on the plates (pictured below).

The dilution scheme was made using an 8-strip of PCR tubes. 90 µL of TSB was placed into 7 of the 8 tubes with a p200 micropipettor. To create a 10-fold dilution in the first tube, 10 µL of high titer lysate was added to the first PCR tube and gently pipetted up and down 10 times. After discarding the tip, a 100-fold dilution was made by taking 10 µL from the first tube and adding it to the second PCR tube and pipetting up and down 10 times. This process was repeated for dilutions 10^{-3}-10^{-7}. By this point, the top agar had solidified. Using the p20 micropipettor, 10 µL of the 10^{-7} dilution was dropped onto the "7" square of the grid. Using the same tip, 10 µL of the 10^{-6} dilution was dropped into the "6" square. The same was done for the remainder of the squares on the grid, maximizing the spacing in between drops to prevent merging. With a fresh tip, 10 µL of the undiluted lysate was placed in the square labeled "0". The lid was replaced slightly askew and plate was placed next to a flame. The drops were allowed to absorb into the agar, which took approximately 45 minutes, and then flipped upside down and placed in the incubator overnight at 37° C.

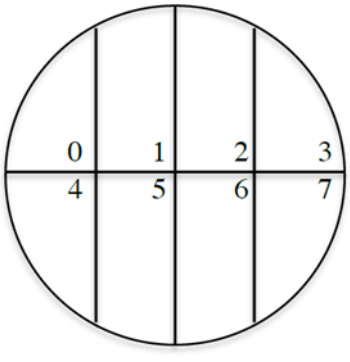

Phage Cleanup and Concentration

Two 50 mL, one 15 mL conical tubes were labeled with date, initials, and "1st high titer lysate". Using aseptic technique, 20 mL of the high titer lysate was placed into each of the 50 mL tubes and ~10 mL was placed into the 15 mL tube. Each student labeled a 1.5 mL microtube with initials, pathogen, phage source, and date, and placed 1 mL of the high-titer phage lysate into their 1.5 mL tube. The tube was then placed into a centrifuge and spun at 24,000 *x g*, 4°C, for 1

hour. During the spin, 10 mL of 0.1 M solution of ammonium acetate was prepared by placing 1 mL of 1 M ammonium acetate and 9 mL of ultra-pure dH_2O into a 15 mL conical tube. Following the first spin, a micropipettor set at 150 µL was used to extract 900 µL of the supernatant from the 1.5 mL tube. Six 150 µL extractions occurred; both the sides and the bottom were avoided. The pellet was then washed with 900 µL of ammonium acetate and inverted 3 times. This centrifugation protocol was repeated 3 times before the phage were treated with DNase I (to remove cell debris).

Electron Microscope Grid Preparation

5 µL of cleaned and purified high titer lysate was placed on a copper EM grid (300 mesh, Formvar-coated) and allowed to absorb into the grid for 5 minutes. Excess liquid was removed from the grid after 5 minutes with a triangular piece of absorbent Whatmann paper. One drop of 2% uranyl acetate solution was placed on top of the grid and allowed to stain the sample for 20 seconds, then was removed using Whatmann paper.

Host Range Analysis

7 TSA+ 5mM $CaCl_2$ plates were prewarmed at 37°C for ~10 min. 7x15ml conical tubes were labeled with initials and host organism. A numbered grid was marked out as in the Titer Assessment protocol. HIA overlays were prepared with 4 mL of HIA top agar, 4 µL 5M $CaCl_2$, and 100 µL of overnight host culture. Immediately after combining components, the tube was inverted 3 times and poured onto the appropriately labeled tube. Allowed plates to set for ~10 min. Prepared 10-fold, 100-fold, 10^{-3}-fold (to 10^{-7}-fold) dilutions and spotted on plates in corresponding squares. Plates sat with lids ajar for ~30 min until dry, then were inverted and placed in incubator overnight at 37°C. (Hosts used: *S. epidermidis RP62a, S. epidermidis 1457, S. aureus ST398, S. aureus Newman, S. pseudointermedius ED99, S. intermedius NCTC11048, S. delphini 8084, S. epidermidis LM1680, S. epidermidis ATCC12228, S. epidermidis 1292*.)

DNA Extraction

Removing contaminating nucleic acids - 20 µL of 10mg/mL RNase A and 4 ul of 50 mg/mL DNase I were added to 2x20 mL aliquots of high titer lysate. Lysates were incubated for 30 min at 37°C in a waterbath. Following incubation, 10 mL of precipitant solution (30% w/v PEG-8000, 3M NaCl) was added to the lysates and tubes were inverted several times. Phage allowed to sit overnight at 4°C.

Concentration of phage pellet - Precipitated lysates were centrifuged for 10 min at 10000xg at 4°C. The supernatant was carefully removed (ALL liquid must be removed before continuing), and the pellets were resuspended in 250 µL of 5mM $MgSO_4$. The resuspended pellets were then transferred to a 1.5mL tube and stored overnight at 4°C.

Proteinase K digestion - 10 µL of 0.5 M EDTA pH 8 and 10 µL of proteinase K (20mg/mL) were added to the resuspended phage and incubated at 50°C for 30 min. Allowed to cool to room temperature for ~10 min.

Phage genome extraction - Promega Wizard DNA cleanup kit used. Purification resin was resuspended and 1 mL was placed in a 1.5 mL microtube. 500µL of the resuspended phage was placed in a 2 mL screw-cap microtube. 1 mL of purification resin was added to the 2 mL microtube, and the tube was inverted gently 5-6 times. A sterile syringe was prepared by attaching a Wizard minicolumn to the barrel and removing the plunger. The phage-resin mixture was then placed in the barrel and pressed through the column over a waste receptacle. The minicolumn was detached and the syringe plunger removed. After reattaching the minicolumn, 2 mL 80% isopropanol was then added to the barrel to wash the column. The lid of a 1.5 mL microtube was cut off and the minicolumn was placed in the top. The tube was centrifuged at 13000xg for 2 min to dry the resin. The minicolumn was then placed in a fresh tube, and 100 µL of 80°C dH_2O was added to elute the nucleic acid. The microcolumn was then centrifuged at 13000xg for 1 min. Using a Nanovue Spectrophotometer, the DNA concentration was calculated and the phage DNA stored at -20°C.

Phage Genome Typing

On ice, 400ng of genome, diH_2O (to reach a nucleic acid+H_2O volume of 8 µL), 1 µL of 10X nuclease buffer, and 1 µL of nuclease (DNase or RNase) or 1µL of diH_2O (NC) was placed into 3x1.5 mL tubes labeled "NC," "R," and "D" for negative control, RNase A, and DNase I. Tubes were incubated for 30 min at 37°C in a heating block. Following the digestion, 1 µL of 0.5 M EDTA and 1 µL of Proteinase K were placed in each tube and allowed to sit for 15 minutes on benchtop. Samples stored at -20°C.

Restriction Enzyme Digest of Genome

On ice, 6 µL of genome, 4 µL of diH_2O, 1 µL of 10X enzyme buffer (RE bf or bf 2.1 for Hind III), and 1 µL of restriction enzyme (Bam HI, Cla I, Eco RI, Hae III, Hind III) or nuclease-free H_2O were combined in the appropriately labeled tubes. All tubes were incubated in a waterbath set to 37°C for 1 hr. The digests were then pulsed in a microcentrifuge and stored at -20°C.

Casting Agarose Gel

500 mL of 1X TAE (Tris-acetate, EDTA) was

prepared by combining 50 mL of 10X TAE and 450 mL of ultrapure dH_2O in a 1 L bottle and swirl until combined. 50 mL of 0.5% agarose gel prepared by combining 0.25g agarose and 50mL of 1X TAE in a flask and heating for 30 seconds 3x or until agarose is melted. 2.5 µL Ethidium bromide was added to the liquid agarose after ~10 min, swirled, and poured into casting apparatus after an additional 5 min. Well comb was inserted and gel allowed to sit for ~30 min until solidified.

Electrophoresis and Imaging

Gel was placed in running apparatus with wells at black electrode and covered in 1X TAE buffer. 3µL of 6X loading buffer was added to each tube and mixed. 5 µL 1kb DNA ladder was loaded into leftmost lane, followed by 10 µL of NC tube, RNase, and DNase tubes. Lid was replaced, corresponding leads attached, and power supply was set to constant 120V. After the gel was allowed to run for 30 min, the power supply was turned off and lid was removed. Gel was removed from running apparatus and was imaged using a UV Light Imager.

Phage Growth Dynamics

1 mL of 1:100 host culture (*S. epidermidis RP62a* or *S. epidermidis ATCC12228*) was placed in 6 tubes (3x15 mL tubes for each host) and labeled in duplicate "0", "1", "5". A volume of lysate with a $5x10^7$ concentration (20 µL) was added to "5" (MOI=5). 4 µL of lysate was placed in "1" (MOI=1, $1x10^7$). 100 µL sterile TSB was added to "0" and 16 µL was added to "1" to make total volumes equal. Into a 96-well plate, 200 µL of sterile TSB was distributed to wells 1-3, 200 µL of "0" was distributed to wells 4-6, 200 µL of "1" was distributed to wells 7-9, and 200 µL of "5" was distributed to wells 10-12. Loading process was repeated for each culture used. Plate was incubated with shaking at 37° C with OD600 readings taken every 15 minutes for 12 hrs.

Results

Plating of TWTP Lysate

After co-culturing with *S. pseudointermedius* ED99, the Tuscaloosa wastewater-derived phage source was plated with a top agar bacterial lawn containing *S. pseudointermedius* ED99. After incubation, the initial plates exhibited no plaques on both the negative control and the experimental sample containing 100 µL of the phage source lysate. A second set of plating showed no plaques when a lysate from Northport Wastewater, co-cultured with *S. epidermidis* RP62a, was combined in a top agar mixture containing *S. pseudointermedius* ED99. Drop dilutions on a fourth plate, from original lysate (from Tuscaloosa Wastewater) to 1:1000 dilution, showed no signs of plaques (**Figure 1**).

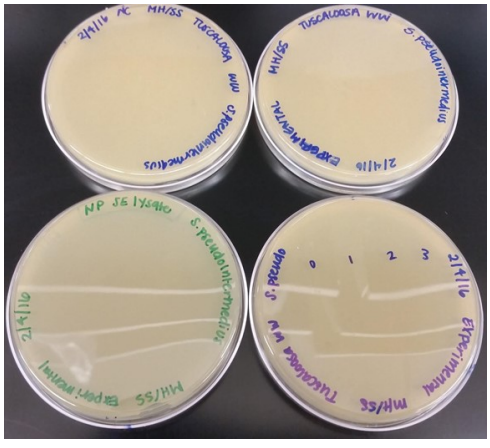

Figure 1. Tuscaloosa wastewater-derived phage source co-cultured with *S. pseudointermedius* ED99, plated on top agar bacterial lawn of *S. pseudointermedius* ED99 (top-right) or with Northport lysate co-cultured with *S. epidermidis* RP26a on *S. pseudointermedius* (bottom-left.) Negative control (top-left) was plated with *S. pseudointermedius* ED99 and sterile TSB instead of lysate. Drop dilutions (bottom-right) and plates exhibited no signs of plaques.

Plating of NPWW Lysate

A new lysate, co-cultured with *S. epidermidis* RP26a and derived from sewage collected from the Northport Wastewater Treatment Plant was plated with a top agar bacterial lawn containing *S. epidermidis* RP26a. After five rounds of plaque-picking and replating, homogeneous plaques were observed to be clear and approximately 0.75 mm in diameter, with a sharp, well-defined edge (**Figure 2**)

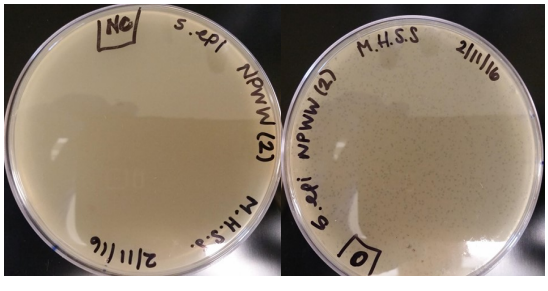

Figure 2. Negative control (left) and undiluted Northport wastewater-derived phage source (right) co-cultured with *S. epidermidis* RP26a, plated on top agar bacterial lawn of *S. epidermidis* RP26a.

High Titer Lysate Concentration

In order to generate a high titer lysate, the phage was propagated in HIA "Sloppy Agar" containing our low titer lysate, *S. epidermidis* RP62a, and 5 mM $CaCl_2$. After releasing the phage into a TSB solution by vortexing, the now *high* titer lysate was filtered and diluted stepwise from original concentration to a $1x10^{-7}$ concentration. 10 µL drops were placed on a top agar bacterial lawn containing *S. epidermidis* RP62a and 5 mM $CaCl_2$ (**Figure 3**). The titer of our high titer lysate was determined to be $8.725x10^9$ PFU/mL ($s=7.14x10^9$) and the titer remains stable in refrigerated storage.

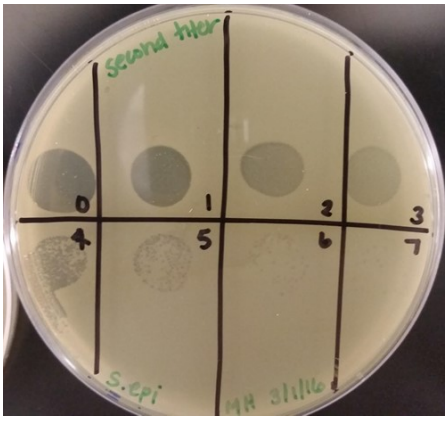

Figure 3. Spotted serial dilutions of high titer lysate. Each spot contained 10 µL of respective serial dilution. (Plate shown = $2.1x10^{10}$ plaque-forming units / mL).

EM Visual Analysis

Transmission electron microscopy shows the phage belonging to the family *Myoviridae*, with a contractile tail and an icosahedral capsid (**Figures 4 and 5**). Genomic typing and capsid size measurements will be performed following the EM imaging.

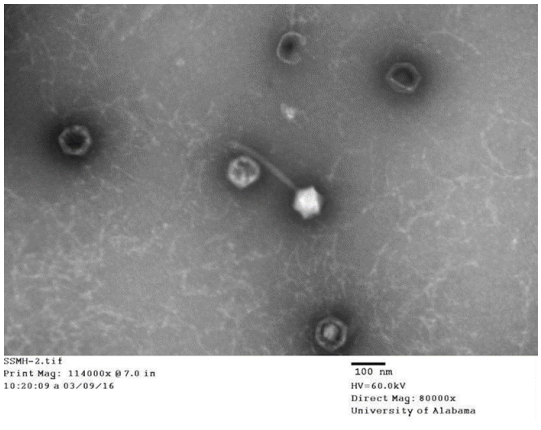

Figure 4. Morphology of isolated phage. Transmission electron micrograph stained with 2% uranyl acetate.

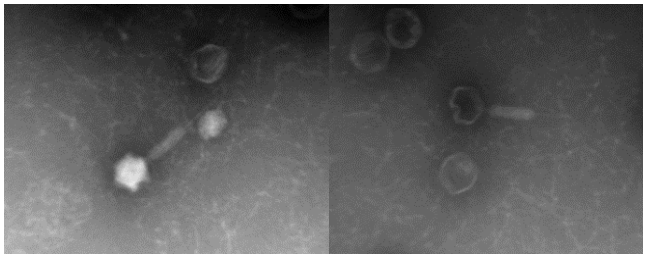

Figure 5. Isolated phage (left) and empty phage (right), both with contracted tails. Transmission electron micrograph stained with 2% uranyl acetate.

Host Range Analysis

Analysis of the host range of the phage was performed with 10 different strains of various Staphylococcal bacteria (**Table 1**). The phage showed considerable plaquing with four of the five strains of *S. epidermidis* used. Lysis from without was also observed with undiluted lysate plated with *S. epidermidis HER 1292* and a 1:10 dilution plated with *S. intermedius.* Other strains showed no plaques in response to lysate exposure.

Host	Strain	Average	STDEV
S. epidermidis	*RP62a*	2.50E+09	6.00E+08
	ATCC12228	2.57E+06	1.40E+06
	1457	4.27E+08	3.33E+08
	*LM1680**	2.60E+08	1.98E+08
	HER 1292	LO 10^0	0
S. aureus	*ST398*	NP	\
	Newman	NP	\
S. pseudointermedius	*ED99*	NP	\
S. intermedius	*NCTC11048*	LO 10^1	0
S. delphini	*8084*	NP	\

Table 1. Host range analysis was performed according to protocol and plaques were counted to the closest value. Phage appears to have specificity for almost every strain of *S. epidermidis* except for HER 1292, where lysis from without was observed. *S. epidermidis RP62a* values taken from most recent lysate. NP= no plaques, LO= lysis from without, *= only two data points were used, \ = no data available.

Phage Genotyping

In order to further characterize our phage, we performed a series of tests to determine the identity of the phage genome and whether it could be cut by restriction enzymes. The following images are 0.5% and 0.7% (respectively) agarose gels on which we ran a nuclease digestion and restriction mapping assay.

A 1 kb ladder and samples of the isolate phage genome,

either uncut or incubated with DNase I or RNase A, were resolved using gel electrophoresis. As seen in **Figure 6**, the genome sample in the presence of DNase I was digested, showing no band on the gel. This is not the the case with the RNase A sample, signifying that the phage genome is of DNA, and not RNA, origin.

Analysis by restriction mapping (**Figure 7**) showed no cutting of the genome by any of the five restriction enzymes used, showing only one band on the gel in the same position as the uncut genome sample. Restriction mapping was repeated with only Eco RI and Hind III, also with no cutting observed.

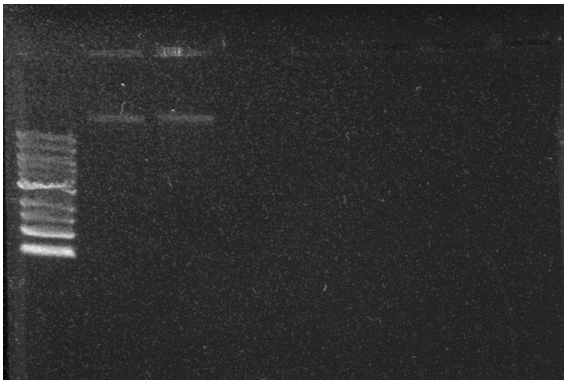

Figure 6- 0.7% agarose gel, (l-r) 1 kb ladder, uncut genome, RNase A, DNase I. Absence of band in DNase well indicates DNA genome.

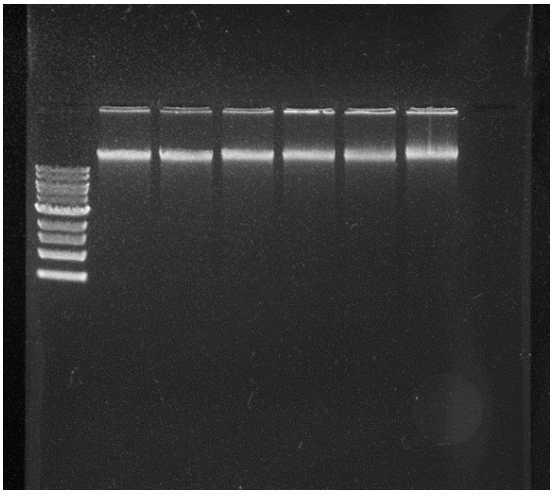

Figure 7. Restriction digest of phage genome. Lane 1-7 from left to right: 1kb ladder, uncut, Bam HI, Cla I, Eco RI, Hae III, Hind III. No cutting and minimal smearing was observed, indicating that our phage is novel and is not cut by any of the usual restriction enzymes.

Phage Growth Dynamics for *S. epidermidis RP62a* and *S. epidermidis ATCC12228*

After observing the efficacy of Mysterymachine against different *S. epidermidis* strains through host range analysis, the study moved forward to a growth dynamics assay to determine whether the Mysterymachine was effective at a MOI of 1 or 5. As a result, we found that both RP62a and ATCC12228 were effectively killed at an MOI of 1 (1:1 ratio of host to phage). For ATCC12228, an MOI=5 killed cells more quickly, but eventually was just as effective as the MOI=1.

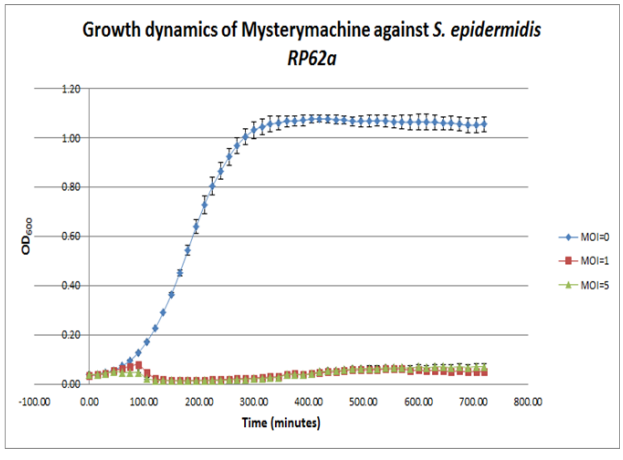

Figure 8. Growth Dynamics of Mysterymachine against RP62a. Efficacy of phage begins at ~100 minutes and continues to suppress the growth of the bacteria at both MOI=1 and MOI=5. Both multiplicities of infection appear to be effective.

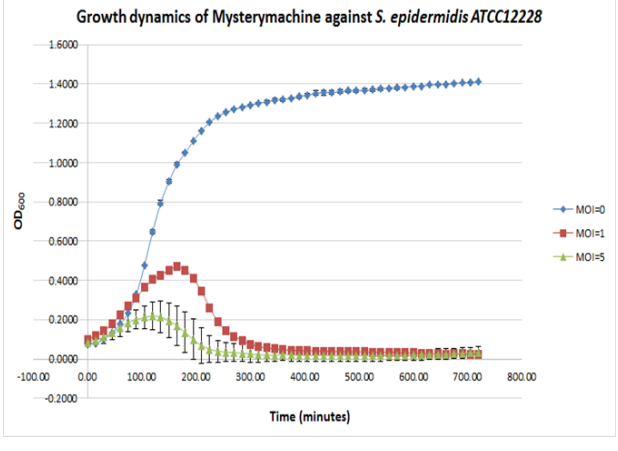

Figure 9. Growth Dynamics of Mysterymachine against ATCC12228. Efficacy of phage begins at ~300 minutes and stabilizes over the remainder of the time course of MOI=1. MOI=5 begins at ~250 minutes, indicating that an MOI=5 is more effective in the beginning of the treatment.

DISCUSSION

Plaque Assay Characteristics

As seen in **Figure 2**, clear, homogeneous plaques were found after 5 rounds plaque-picking and replating. These plaques were approximately 0.75 mm in diameter, with a sharp, well-defined edge. These characteristics can be used as an indication of potential phage traits. For example, the size of the plaque can be influenced by many factors, including but not limited to: adsorption rate, burst size, latent period, and rate of diffusion through top agar of phage [11]. The plaques in this work had a diameter of ~0.75mm, but the mentioned characteristics about the phage itself cannot be determined from this value until further targeted studies, such as a one-step growth curve, have been completed. Additionally, the opacity of plaques can be an indicator of phage virulence. Lytic phages often produce clear plaques, while temperate phages that exhibit lysogenic activity may produce turbid plaques, usually caused by many phages residing within their hosts' genomes, rather than lysing the bacteria [11]. The plaques in this work are clear, indicating that the isolated phage exhibits lytic activity and most likely is virulent. This is confirmed by **Figure 4** that shows the phage is from the family *Myoviridae*, since phages from this family tend to exhibit virulent behavior [12]. Lastly, the clarity of the border of a plaque can yield information as to the presence of released lytic enzymes after initial infection burst. If a plaque has a fuzzy border or a "halo," this may be caused by diffusion of these lytic enzymes away from the initial infection site, continuing to kill periphery host cells [11]. The plaques in this work have a clear, well-defined border with no halo, so it is unlikely that this phenomenon is taking place in the phage present.

TEM Analysis

TEM visualization showed phage present with tails. Upon further analysis, some phage exhibit the presence of tails contracted into a needle-like structure, as seen in **Figure 5**. These details are characteristic of myophages, which can contract their tails to insert their DNA genome into a host cell. Myophages are generally virulent, lysing their host through the lytic pathway [12].

Host Range Analysis

The phage showed considerable plaquing with most of the *S. epidermidis* strains used (**Table 1**). Because of this phage's lytic nature and the fact that it was co-cultured with *S. epidermidis* RP62a during isolation, it is not unexpected that it is most active against these strains. The strains showing plaques possess a receptor recognized by the phage for lytic infection.

Two other strains, *S. epidermidis HER 1292* and *S. intermedius,* showed vague clearing and high concentrations of applied phage lysate. This "lysis from without" may be caused by phage lysins or an abortive infection defense specific to those strains, causing the vague clearing instead of the distinct plaques shown in **Figure 2**. Considering the host range in a therapeutic context, if this phage were considered suitable for such an application, target strains should be considered limited to *S. epidermidis* strains.

Genomic Analysis

Genomic analysis (**Figures 6 and 7**) of the phage revealed DNA origin. This is consistent with Staphylococcal phages from the family *Myoviridae*, which have double-stranded DNA genomes [7]. However, the results of the restriction mapping assay is intriguing. Myophages from the Hatoum-Aslan lab have shown to contain recognition sequences cut by a least one of the restriction enzymes used, especially Eco RI and Hind III. This phage was not cut by any of the restriction enzymes used, confirmed by an experimental replicate using Eco RI and Hind III specifically. It can be reasoned that the genome does not contain any of the recognition sequences cut by these enzymes, but until full genome sequencing is performed, we are unable to be certain of this fact.

Growth Dynamics Analysis

The phage is effective against both *S. epidermidis* RP62a and *S. epidermidis* ATCC12228 (**Figures 8 and 9)**. When unchallenged, both cultures grow exponentially and reach a large population size. However, when a MOI of one phage per bacterium is introduced, the growth of bacteria is reduced dramatically until no bacteria remain. An MOI of 5 shows an even more pronounced trend of growth decline. In comparison, the phage shows higher effectiveness and faster growth disruption against RP62a than ATCC12228.

ACKNOWLEDGEMENTS

The authors of this report would like to thank Dr. Asma Hatoum-Aslan, Dr. Kimberly Lackey, the University of Alabama, the Tuscaloosa Wastewater Treatment Plant, and the Northport Wastewater Treatment Plant for supplying guidance, resources, and equipment for our investigation.

.

References

[1] von Eiff C, Peters G, & Heilmann C. (2002). Pathogenesis of infections due to coagulase-negative staphylococci. Lancet Infect Dis. 2002 Nov;2(11):677-85. DOI: 10.1016/S1473-3099(02)00438-3

[2] Otto M. (2009). Staphylococcus epidermidis--the 'accidental' pathogen. Nat. Rev. Microbiol. 7 555–567.

[3] Namvar AE, Bastarahang S, Abbasi N, Ghehi GS, Farhadbakhtiarian S, Arezi P, Hosseini M, Baravati SZ, Jokar Z, & Chermahin SG. Clinical characteristics of Staphylococcus epidermidis: a systematic review. GMS Hyg Infect Control. 2014;9(3):Doc23. DOI: 10.3205/dgkh000243, URN: urn:nbn:de:0183-dgkh0002436

[4] Büttner H, Mack D, & Rohde H. (2015). Structural basis of Staphylococcus epidermidis biofilm formation: mechanisms and molecular interactions. Front. Cell. Infect. Microbiol. 5:14. doi: 10.3389/fcimb.2015.00014

[5] Cerca N, Martins S, Cerca F, Jefferson KK, Pier GB, Oliveira R, & Azeredo J. (2005). Comparative assessment of antibiotic susceptibility of coagulase-negative staphylococci in biofilm versus planktonic culture as assessed by bacterial enumeration or rapid XTT colorimetry. J Antimicrob Chemother 56, 331–336.

[6] Sulakvelidze A, Alavidze Z, & Morris Jr. JG. (2001). "Bacteriophage therapy," Antimicrobial Agents and Chemotherapy, vol. 45, no. 3,pp. 649–659, 2001.

[7] Elbreki M, Ross J, Hill C, O'Mahony J, McAuliffe O, & Coffey A (2014). Bacteriophages and Their Derivatives as Biotherapeutic Agents in Disease Prevention and Treatment. *Journal of Viruses,* vol. 2014, Article ID 382539

[8] Kutateladze M & Adamia R. (2010). Bacteriophages as potential new therapeutics to replace or supplement antibiotics. Trends Biotechnol 28, 591–595.

[9] Loc-Carrillo C & Abedon ST. (2011). Pros and cons of phage therapy. Bacteriophage 1, 111–114.

[10]Melo L, Sillankorva S, Ackermann H, Kropinski A, Azeredo J, & Cerca N. (2014). Isolation and characterization of a new Staphylococcus epidermidis broad-spectrum bacteriophage. *Journal of General Virology*, 95, 506–515

[11] Gallet R, Kannoly S, and Wang IN. (2011). Effects of bacteriophage traits on plaque formation. BMC Microbiol. 11:181, 1-16

[12] Deghorian M & Van Melderen L. (2012). The Staphylococci Phages Family: An Overview. Viruses. 4, 3316-3335

The Role of miRNA in Dopamine Synthesis and Signaling

Samuel P. Stanley

Faculty Mentor: Dr. Kim Caldwell
Department of Biology, The University of Alabama, Tuscaloosa, AL 35487

Dopamine is a well-studied neurotransmitter associated with motor function and reward. Following synthesis, dopamine also acts as a precursor of other catecholamines. miRNAs are a class of small, non-coding RNA molecules known to play significant roles in gene expression. peripheral nervous system and at neuromuscular junctions throughout the body. Following cleavage, mature miRNAs bind to specific mRNAs and inhibit particular genetic elements by inducing cleavage or general degradation. miRNAs have been found to regulate the development and function of dopamine neurons, particularly through the Pitx3 feedback loop. In this, miRNA-133b is important in regulating dopamine neuron differentiation and is shown to be responsive to extracellular stimuli. miRNA-132 is also associated with dopamine neuron development through regulation of Nurr1 expression. Finally, miRNA-504 is shown to regulate dopamine neuron function through allelic regulation of the Dopamine Receptor D1. While the full relationship between miRNA regulation and dopamine neuron health has yet to be fully explored, there exists significant evidence pointing to extensive regulation of dopaminergic elements by a variety of miRNAs.

Introduction.

The neurotransmitter dopamine is known to be instrumental in reward and movement regulation in the brain. Dysfunction of the dopamine signaling system has been associated with a number of nervous system diseases, including Parkinson's disease and the aptly named dopamine dysregulation syndrome. Although a number of cellular mechanisms regulating dopamine synthesis, secretion, and reuptake at a transcriptional level have been identified, there remains relatively little published work on post-transcriptional regulatory mechanisms. MicroRNAs (miRNAs) are an increasingly studied mechanism of post-transcriptional repression known to be vital for maintaining cellular homeostasis. Though the role of miRNAs in regulating the synthesis of dopamine and dopamine related machinery remains understudied, an increasing number of publications have alluded towards a dynamic, highly complex series of mechanisms behind both miRNA and miRNA target regulation. This analysis will delve into some of these publications and, particularly, will attempt to highlight the number of and mechanisms by which miRNAs regulate dopaminergic activity. While there will be limited discussion on the role of specific complexes in general dopamine and miRNA function, the primary purpose of this analysis is to examine the relationship between known miRNAs and dopamine signaling.

Dopamine Synthesis and Signaling Basics.

Dopamine is one of the most well studied neurotransmitters and is associated with a broad variety of neurological functions. When associated with motor function, the molecule is produced in the dopamine neurons of the substantia nigra from where it is discharged into the striatum. When associated with reward, dopamine is produced in nerve cell bodies of the ventral tegmental area and is released into the prefrontal cortex and nucleus accumbens. Curiously, dopamine itself isn't only an end state. Rather, the molecule acts as a precursor in the synthesis of other catecholamines such as norepinephrine and epinephrine on top of its role as a neurotransmitter [1]. Regardless of where it's physically synthesized in humans or what its final state is destined to be, the machinery behind dopamine synthesis remains unchanged. Beginning with the dopamine precursor L-Tyrosine, the molecular precursor of dopamine, is first acted upon by tyrosine hydroxylase, converting it to L-DOPA. Tyrosine hydroxylase is known to be the rate-limiting enzyme in the catecholamine synthesis pathway [2] and, thus, is the target of many pharmaceuticals hoping to bolster dopamine synthesis. L-DOPA is next acted upon by DOPA decarboxylase and Aromatic L-amino acid decarboxylase, yielding dopamine and CO_2. From here, the dopamine molecule can either be used directly as a neurotransmitter or, alternatively, can be acted upon by Dopamine β-hydroxylase to begin its conversion to norepinephrine or epinephrine [1].

As a neurotransmitter, dopamine is released from the presynaptic terminal of a dopamine neuron into the synapse via synaptic vesicles. The dopamine molecules rapidly cross the synapse and are recognized by a number of dopamine receptors along the surface of the postsynaptic terminal. This signal is then propagated down a line of neurons, eventually yielding an appropriate response. Synaptic dopamine, while initiating this postsynaptic response, also serves to inhibit the release of further dopamine from the presynaptic cell by binding to presynaptic dopamine receptors. These presynaptic bindings are also capable of inhibiting further synthesis of dopamine in the presynaptic cell and serve to maintain intracellular dopamine levels [13]. Thus, dopamine receptors play an important role in both propagating a particular signal and maintaining neurotransmitter homeostasis both in and out of the cell.

After fulfilling its purposes in the synapse, dopamine is reuptaken into the cytosol. This is accomplished through either plasma membrane monoamine transporters or, more commonly, relatively high-affinity dopamine transporters. Once inside the cytosol, the dopamine molecules are repackaged into vesicles via vesicular monoamine transporter 2 or, if synaptic levels of dopamine are critically low, are output back into the synapse via the reverse actions of the dopamine transporter [14]. In all, dopamine signaling on a cellular level is dynamic in nature and is reliant at a molecular level on dopamine receptors, dopamine transporters, and vesicular transporters.

miRNA Basics.

miRNAs are a class of 21-23 nucleotide, non-coding RNA molecules that are known to play significant regulatory roles in gene expression. miRNAs act through mRNA inhibition, wherein an miRNA will bind to a site specific "seed region" of an mRNA's 3' untranslated region (3'UTR) and cause it to undergo either cleavage or generalized degradation [3]. While the complete synthesis and processing pathways of miRNAs are still being explored, the core elements of miRNA production are similar to other RNA synthesis pathways in nature. Briefly, large precursor miRNAs known as pri-miRNAs are transcribed and cleaved into pre-miRNAs in the nucleus by the Drosha complex before being exported to the cytosol via Exportin-5. Once in the cytosol, the pre-miRNAs are processed by the Dicer complex into double stranded miRNAs. One of these strands is detached and degraded, yielding the remaining strand as a mature miRNA [4]. This miRNA will then bind to an mRNA as described above and inhibit a particular genetic element. It's worth noting that, while seed sites are inherently short due to the nature of miRNA length, miRNA inhibition is highly selective and is regulated by both internal and external cellular factors.

miRNAs Regulate the Development and Function of Dopamine Neurons.

Parkinson's disease, while best known for its signature locomotive manifestations, is defined clinically as a loss of dopamine neuron function within a region of the midbrain known as the substantia nigra. While a number of transcription factors have been found to influence dopamine neuron development, function, and longevity [5], relatively little is known about the role of posttranscriptional regulatory mechanisms in maintaining neuron health. Kim *et al* [6] explored the role of miRNAs in dopamine neuron development using murine embryonic stem cells conditionally expressing Dicer. Using a standard embryoid body protocol, the cultures were differentiated to a midbrain dopamine neuron phenotype, allowing for observation on the functions of miRNA as the dopamine neurons developed. Dicer knockout in these lines was observed to significantly decrease the ability of stem cells to successfully differentiate into dopamine neurons relative to functional Dicer controls. Furthermore, supplementation of small RNA molecules extracted from embryonic mouse midbrains was found to rescue from this loss, suggesting that Dicer dependent expression of miRNA is critical in midbrain dopamine neuron development and longevity. Dicer depletion was subsequently carried out in intact rodent central nervous systems, where similar neuronal health results were observed. Importantly, locomotive phenotypes reminiscent of those associated with Parkinson's disease were observed in Dicer knockout animals, suggesting that miRNA function is essential for the maintenance of a variety of neuron types including dopamine neurons. The investigators further identified miRNA-133b as a key component of the paired-like homeodomain transcription factor Pituitary homeobox 3 (*Pitx3*) feedback loop within dopamine neurons, showing that individual miRNAs have highly specific roles in the dynamic systems responsible for keeping dopamine neurons intact. Furthermore, changes in the *Pitx3* feedback loop were found to affect the expression levels of tyrosine hydroxylase [7], and the dopamine transporter [8]. In all, the findings of Kim *et al*. demonstrate the broader role of miRNA in dopamine neuron health and highlight the importance of individual miRNAs in regulating the machinery behind dopamine signaling.

The miRNA-133b Pitx3 Feedback Loop is Important in Dopamine Neuron Differentiation and Function.

As the essential nature of miRNA-133b in dopamine neuron function was established in 2007, several teams proceeded to investigate how it specifically modulated dopamine signaling in the following years. Sanchez-Simon *et al* [9] published first on the matter, examining the mechanism by which opioids affect midbrain dopaminergic neurons via the miRNA-133b *Pitx3* feedback loop. The team observed that embryonic exposure to opioids in zebrafish led to the decreased expression of a number of miRNAs including miRNA-133b within developing neurons. These shifts corresponded to changes in tyrosine hydroxylase and dopamine transporter levels which, as *Pitx3* is known to positively regulate the synthesis of both [10], was expected. Interestingly, these results were unique to immature neurons, suggesting that control of miRNA-133b activity is developmentally dependent. Further analysis revealed that morphine, a common opioid, regulated miRNA-133b levels via activation of the opioid receptor. In all, these results suggest that extracellular regulation of the miRNA-133b *pitx3* feedback loop is both specific and temporal which, in the context of broader dopamine signaling, alludes towards dynamic regulatory mechanisms as an organism matures.

Additional characterization of the relationship between miRNA-133b, *Pitx3*, and some of the key machinery behind dopamine signaling was performed by Barreto-Valer *et al* [11]. Using zebrafish embryos, the team determined that embryonic exposure to cocaine resulted in

lowered central nervous system and peripheral nervous system levels of miRNA-133b. This corresponded to an increase in *Pitx3* and *Pitx3* target expression. To confirm the inhibitory nature of miRNA-133b on *Pitx3* more directly, the team introduced 3'UTR Modified-*Pitx3* to their subjects, effectively preventing miRNA silencing of the new molecules. These animals produced phenotypes similar to those wherein miRNA-133b had been downregulated by cocaine, providing evidence that the miRNA-133b *Pitx3* feedback loop is responsible for modulating the expression of several key elements of the dopamine signaling system at a cellular level. Of note, the team also observed that *Pitx3* expression led to increased expression of dopamine receptor Drd2a and decreased expression of dopamine receptor Drd2b. This suggests that the miRNA-133b *Pitx3* feedback loop is more extensive in dopamine signaling than initially hypothesized.

miRNA-132 Regulates the Development of Dopaminergic Neurons.

As a number of miRNAs have potential for dopamine regulatory activity, Yang *et al* [12] explored the role of miRNA-132 in neuron differentiation. Utilizing tyrosine hydroxlase driven fluorescence-activated cell sorting and subsequent miRNA profiling, the team generated relative miRNA expression profiles for dopamine and non-dopamine neurons. Through this, they identified miRNA-132 as a dopamine neuron preferentially expressed molecule. Subsequent bioinformatic analysis revealed that miRNA-132 was predicted to interact with a seed sequence on the Nurr1 mRNA molecule. The Nurr1 protein itself is well-established as a key transcription factor in dopamine neuron development as it induces tyrosine hydroxylase expression and is known to interact with *Pitx3*. The team next utilized a series of overexpression and underexpression assays in conjunction with luciferase tagged Nurr1 to determine that miRNA-132 does, in fact, modulate Nurr1 expression. Phenotypically, overexpression of miRNA-132 led to inhibited neuronal differentiation whereas usage of miRNA sponges in overexpression lines resulted in mild rescue from this condition. Measuring the relative levels of Nurr1, miRNA-132, and Nurr1 products, the team determined that the expression of all three listed elements changes significantly over time. Of note, levels of Nurr1 and miRNA-132 expression remained tied together, as the repression of Nurr1 inhibited the expression of miRNA-132 and vice versa. Thus, these data suggest that there exists at least one feedback mechanism whereby developing neurons rely on miRNA inhibition to avoid specific forms of protein overexpression and that this mechanism is dynamic in nature. Furthermore, these findings show that the dopamine regulatory system has a complex series of cellular controls that manage not only the initiation and maintenance of dopamine homeostasis but the proteostasis of the machinery responsible for the dopamine system itself.

miRNA-504 Modulates Differential Allelic Expression of Dopamine Receptor D1.

While miRNA inhibition is known to regulate the expression of many wild-type dopamine related genes, there exists evidence to suggest that miRNA activity also leads to differences in allelic expression. Point mutations in the gene encoding dopamine receptor D1 have previously been shown to modify organism preference towards addictive behaviors. Curiously, these point mutations appear out of the protein coding domain of the gene and are associated with shifts in gene product expression [15]. Huang *et al* [16] characterized the mechanism by which this allelic differentiation occurs, finding that miRNA-504 actually serves to enhance dopamine receptor D1 expression. Utilizing a bioinformatic screen, the group first determined that miRNA-504 was predicted to target the 3'UTR of dopamine receptor D1 bearing one of two point mutation phenotypes. While another miRNA (miRNA-296) demonstrated preferable binding potential to one of the two point mutations, miRNA-504 is known to be relatively highly expressed in the brain and, in preliminary assays, was found to have a more profound effect on protein expression. Proceeding with miRNA-504 analysis, the investigators next utilized a series of miRNA-504 mimics and inhibitors, observing the relative expression levels of the two alleles. Through these experiments, it was observed that miRNA-504 effectively modulated the relative expression of the two alleles, leading to functional differences in the levels of protein product from each. From a practical standpoint, this would lead to areas of altered dopamine receptor D1 density throughout the brain and would likely lead to dysregulation of dopamine homeostasis. These altered expression levels were thought to be due to differences in miRNA-504 seed site affinity and are in line with the results predicted by the aforementioned bioinformatic approach. Importantly, these changes in expression were opposite what one would expect if miRNA-504 was inhibiting the dopamine receptor D1 allele it demonstrated a high affinity towards. Further experimentation found that reduced levels of miRNA-504 led to a decrease in dopamine receptor D1 expression while a miRNA-504 mimic led to an increase. The same was observed with the low-affinity allele, albeit to a lower degree. This data, remarkably, suggests that miRNA function can lead to expression upregulation and that, in this case, miRNA-504 induced upregulation is responsible for increases in dopamine receptor D1 expression. While prior evidence of miRNA upregulation existed prior [17] to Huang *et al* [16], dopamine system specific miRNA upregulation had yet to be discovered. Further investigations have since revealed that miRNA upregulation events are highly mRNA specific and, while important, are rare relative to miRNA posttranscriptional repression activity [18].

Concluding Remarks.

Regulation of dopamine synthesis and signaling is high-

ly complex at the cellular level. While the transcriptional and posttranslational mechanisms by which dopamine is regulated are relatively well understood, the posttranscriptional regulatory means have yet to be well explored. miRNAs 133b, 132, and 504 are all associated with different levels of dopamine synthesis or signaling and vary tremendously in the means by which their regulation is carried out. The diversity of feedback mechanisms by which gene products and their inhibitory miRNAs are dynamically expressed add tremendously to the already complex circuitry behind dopamine signaling. Regardless of whether they inhibit or enhance protein expression, these miRNAs are crucial for developing and maintaining dopamine homeostasis and, along with a number of transcriptional and posttranslational mechanisms, form the backbone of dopaminergic health.

miRNAs represent an important yet understudied element of neurotransmitter regulation at the cellular level. While an increasing number of studies have emerged in recent years exploring the roles of particular miRNAs in dopamine synthesis and signaling, the sheer number of completely unanalyzed miRNAs with the potential to impact dopaminergic activity only highlights the need for further research in the field. Particularly, given the conserved nature of the many pathways by which dopamine regulating miRNAs are themselves regulated, examining the role of these miRNAs at a basic level are amenable to most model organisms and highly relevant for better understanding human health. In this sense, miRNAs possess significant potential for illuminating the elusive gene-by environment interactions associated with a number of important human diseases including Parkinson's Disease.

References:

[1] H. Olguin, D. Guzman, E. Hernandez-Garcia, G. Mejia (2016). The Role of Dopamine and Its Dysfunction as a Consequence of Oxidative Stress. Oxidative Med and Cellular Longevity. 13.

[2] K. Mizuno, J. Kawatani, K. Tajima, A. Sasaki, T. Yoneda, M. Komi, T. Hirai, A. Tomoda, T. Joudoi, Y. Watanabe (2016) Low putamen activity associated with poor reward sensitivity in childhood CFS. Neuroimage. 12. 600 .

[3] P. Nelson, M. Kiriakidou, A. Sharma, E. Maniataki, Z. Mourelatos (2003) The microRNA world: small is mighty. Trends Biochem Sci. 28. 534.

[4] J. Weber, D. Baxter, S. Zhang, D. Huang, K. Huang, M. Lee, D. Galas, K. Wang (2010) The microRNA spectrum in 12 body fluids. Clin Chem. 56. 1733.

[5] A. Wallen, T. Perlmann, Ann. (2003) Transcriptional control of dopamine neuron development. N. Y. Acad. Sci. 991. 48.

[6] J. Kim, K. Inoue, J. Ishii, W. Vanti, S. Voronov, E. Murchison, G. Hannon, A. Abeliovich (2007) A microRNA feedback circuit in midbrain dopamine neurons. Science. 317. 1220.

[7] S. Daubner, T. Le, S. Wang (2010) Tyrosine Hydroxylase and Regulation of Dopamine Synthesis. Arch. Biochem. Biophys. 508. 1.

[8] G. Miller, R. Gainetdinov, A. Levey, M. Caron (1999) Dopamine transporters and neuronal injury. Trends in Pharma. Sciences. 20. 424.

[9] F. Sanchez-Simon, X. Zhang, H. Loh, P. Law, R. Rodriguez (2010) Morphine Regulates Dopaminergic Neuron Differentiation via miR-133b Molec. Pharma. 78. 935.

[10] F. Jacobs, S. van Erp, A. van der Linden, L. von Oerthel, J. Burbach, M. Smidt (2009) Pitx3 potentiates Nurr1 in dopamine neuron terminal differentiation through release of SMRT-mediated repression. Development. 136. 531.

[11] K. Barreto-Valer, R. Lopez-Bellido, F. Sanchez-Simon, R. Rodriguez (2012) Modulation by Cocaine of Dopamine Receptors through miRNA-133b in Zebrafish Embryos. PLOS One. 7(12). e52701.

[12] D. Yang, T. Li, Y. Wang, Y. Tang, H. Cui, Y, Tang, X. Zhang, D. Chen, N. Shen, W. Le (2011) miR-132 regulates the differentiation of dopamine neurons by directly targeting Nurr1 expression. Journal of Cell Science. 125. 1673.

[13] S. Steffensen, K. Bradley, D. Hansen, J. Wilcox, R. Wilcox, D. Allison, C. Merrill, J. Edwards (2010) The role of connexin-36 gap junctions in alcohol intoxication and consumption. Synapse. 65. 695.

[14] K. Schmitt, R. Rothman, M. Reith (2013) Nonclassical Pharmacology of the Dopamine Transportr: Atypical Inhibitors, Allosteric Modulators, and Partial Substraes. Journal of Pharma and Experimental Therapeutics. 346. 2.

[15] W. Huang, J. Ma, T. Payne, J. Beuten, R. Dupont, M. Li (2005) Significant association of DRD1 with nicotine dependence. Cell. 120. 15.

[16] W. Huang, M. Li (2009). Differential allelic expression of dopamine D1 receptor gene (DRD1) is modulated by microRNA miR-504. Biological Psychiatry. 65. 702.

[17] S. Vasudevan, Y. Tong, J. Steitz (2007) Switching from repression to activation: microRNAs can upregulate translation. Science. 318. 1931.

[18] A. Orang, R. Safaralizadeh, M. Kazemzadeh-Bavili (2014) Mechanisms of miRNA-Mediated Gene Regulation from Common Downregulation to mRNA-Specific Upregulation. International Journal of Genomic. 2014. 15.

The Emerging Scholars Program is an exciting opportunity for students at the University of Alabama that helps them get involved in research with a faculty member in their chosen field. The program connects students with world class scientists and gives them the chance to perform research with substantial impacts. Here, we showcase the work of some of our Emerging Scholars to demonstrate a small sample of the fields available to members of the program. We wish all of these young scientists the absolute best as they continue on in their careers.

Elisheba Mann, Chemical Engineering

Faculty Mentor: Dr. David Nikles

I am working to create a magnetically triggered drug release system that delivers needed drugs to cancer patients. We believe the result of this project will exponentially decrease the side effects of cancer treatment and allow doctors to specially target cancer cells.

Lauren Cook, Biology

Faculty Mentor: Dr. Guy Caldwell

Aging is an important risk factor for many diseases, including Parkinson's disease (PD), as the decline of many physiological processes, and the onset of diseases, occurs over time. PD is characterized by the loss of dopaminergic neurons due to the accumulation of the α-synuclein (α-syn) protein that aggregates in and around the neurons. The roundworm, *Caenorhabditis elegans* is a valuable model organism for identifying genetic regulatory mechanisms of aging and longevity. In order to study PD, we have established a model in *C. elegans* by expressing human α-syn in the dopaminergic neurons; this causes these cells to degenerate as the worms age. We have used this model to identify genetic factors, shared between worms and humans, which are inherently neuroprotective and either impacted by or resistant to aging. Previous research identified *nceh-1* in a screen for genes that modulated aging and α-syn-induced dopamine neuron degeneration. Cholesterol is not only an essential structural component for cellular membranes but also required for synapse formation. Thus we are investigating its implications in cholesterol metabolism in respect to α-syn induced neurodegeneration and overall health in the *C. elegans* model of PD.

Evan Pickard, Economics

Faculty Mentor: Dr. Paul Pecorino

The main objective of this project is to determine if there is a certain healthcare model the United States should try to imitate for their healthcare system. With the recent election of Donald Trump and the potential repeal of The Affordable Care Act, this could be a crucial issue to have insight into. We are exploring this through a multiple regressions model that is assessing the Gini Index (disparity in income in a country), life expectancy and GDP per capital across countries categorized in each of the different healthcare models (Bismarck, Beveridge, NHI, Out of pocket model, United States which is a variety). This will give us a negative or positive association among each factor included to each study and how they affect each model.

Madeline Shay, Microbiology

Faculty Mentor: Dr. Kim Caldwell

We are examining the impact of SHMT-1, an enzyme involved in one-carbon metabolism, on the aging process and its possible contributions to disease pathology. We hypothesize that this plays a role in neuroprotection during the aging process. We are utilizing the nematode C. elegans as a model for this study, as this nematode possesses a homolog of the human SHMT gene. The analysis of these results may provide greater insight into the genes involved in Alzheimer's disease in humans and their relation to aging.

Alaric Rohl, Mathematics

Faculty Mentor: Amir Zaheri

Dr. Zaheri and I are attempting to analyze irrational numbers from a music theorist's perspective. We are creating algorithms to convert the digits of an irrational number into hertz values which become musical scales. From here, we look at the relationships between the notes created for each digit in an attempt to reverse engineer properties about the irrational number that might not otherwise be obvious.

Emerging Scholars

Kasie Coogan, Chemical Engineering

Faculty Mentor: Dr. Shreyas Rao

As a part of the Rao laboratory, my current project involves investigating the role of stiffness on the behavior of metastatic breast cancer cells using hydrogel materials. The goal of this research is to most appropriately mimic key aspects of the cancer microenvironment to understand the mechanisms associated with cancer progression. In doing so, we hope to better develop in vitro methods for studying the behavior of these cancer cells and eventually developing better treatment approaches.

Sai Dwarampudi, Biology

Faculty Mentors: Dr. Kristina McDonald & Dr. Stephen Ungvary

My work explores the role of physiological processes in psychopathy specifically through the lenses of callous and unemotional traits, narcissism, and impulsivity in relation to heart rate, vagal tone, and heart rate and vagal reactivity (combined).

Kaitlin Burnash, Chemical Engineering

Faculty Mentor: Dr. Mary Kay Meyer

Our objective is to investigate the effects that culture and family upbringing play in the formation of body image in young adults. Every culture sends subliminal and obvious messages to young adults that can dramatically affect the formation of one's first ideal body image. These ideal body images are indicators of long-term happiness and success in everyday life. In particular, certain cultures glorify an extremely thin body ideal while others glorify a much thicker body ideal, both of which are unhealthy from a biological standpoint.

Sean Drummond, Biology

Faculty Mentor: Dr. Stephen Secor

I am working on a project in Dr. Secor's lab to examine the role of intestinal metabolism in maintaining blood glucose homeostasis. Diabetics who undergo gastric bypass surgery as a means to lose weight experience in a relatively short time a decrease in blood glucose and the restoration of glycemic control. It has been demonstrated with gastric bypass mice that the surgically re-routed small intestine experiences tissue remodeling and an increase in glucose metabolism. Therefore suggested is that the altered intestine becomes a sink for ingested glucose resulting in a lowering of blood glucose levels. We are exploring the extent that an active intestine utilizes glucose using the diamondback water snake. Snakes normally experience a dramatic increase in intestinal glucose metabolism and no change in blood glucose levels during meal digestion. We are testing this hypothesis by administering a glucose load to snakes and after their blood glucose has begun to increase, the snakes are then fed. If blood glucose drops to normal levels after feeding, this would support the hypothesis that active digestive tissues can rapidly utilize ingested glucose and thus reduce the incidence of hyperglycemia.

Adam Holzhauer, Microbiology

Faculty Mentor: Dr. Guy Caldwell

Our research investigates genetic pathways for resilience to proteotoxic stress in the nematode *C. elegans*. Initial data has been collected in a Huntington's Disease model utilizing a mutant strain expressing a temperature sensitive dynamin variant (which shuts down dynamin activity at 25 C) as a means of selecting for resilience. We are currently working on utilizing the same methods to select for resilience in a Parkinson's Disease model. Ultimately, we intend to discover the pathway by which resilience is established in these animals.

Stanislava Chtarbanova-Rudloff, PhD
Assistant Professor
Department of Biological Sciences, University of Alabama

Dr. Chtarbanova-Rudloff is a newly arrived faculty member at the University of Alabama. In this new segment about UA faculty, JOSHUA spoke to Dr. Chtarbanova-Rudloff about her background, her research interests, and her advice for young scientists.

Sam Scopel: With regards to your background, would you mind taking us through what eventually led you to the University of Alabama? For example, where are you from and what did you do prior to joining the faculty here?

Stanislava Chtarbanova-Rudloff: I grew up in Bulgaria and attended high school in Sofia. After graduating from high school I went to college in Strasbourg (France), where I got my BS in Biochemistry, MS in Immunology and PhD in Cellular and Molecular Biology. My studies in graduate school focused on the anti viral immune response and the pathogenesis of viral infection in the fruit fly Drosophila. After that I moved to Madison for a postdoctoral training at the University of Wisconsin where I studied the involvement of the immune system in neurodegeneration again using the fly as an experimental model. Then, I accepted a position in Tuscaloosa and joined the University of Alabama as an assistant professor of cellular and molecular immunology.

SS: What would you say is the primary focus of your research?

SCR: The primary focus of my research is to understand the mechanisms that underlie the aging of the innate immune system and the ones that mediate immune reactions in the brain. Aging is accompanied by several physiological changes, including changes in the functioning of the immune system. For example, aging is associated with increased inflammation that can contribute to or can exacerbate other age-dependent pathologies such as cancer or neurodegenerative diseases. We have an uncomplete understanding of the factors that contribute to this inflammatory status and one of our goals is to gain further knowledge about this process. It is also well known that the organismal ability to fight infections declines with age. This is another area of research that we are working on in the lab: we are looking to discover novel factors that play a role in fighting infections in the aging organism. Additionally, we are also trying to gain a better understanding of the innate immune system activation in the brain following infection with bacteria or viruses.

SS: And why, out of all the questions yet to be answered within the field of biology, do you feel compelled to tackle this one? What draws you to this area of study?

SCR: It is definitively my strong interest in immunology and specifically in the innate immune system. I developed a strong interest in immunology when I was an undergraduate student and then was able to pursue my PhD in the field of innate immunity at the University of Strasbourg where I worked on innate immune defenses against viruses. I was always fascinated by the complexity of this system and how all aspects of the immune response have to be tightly regulated in order to assure proper functioning to protect the body from harmful invaders. If immune reactions persist for too long, then this can lead to negative outcomes and result in disease. In the recent years, chronic inflammation appears to be associated with almost all age-related disorders and I found it particularly appealing to be able to contribute to that field.

SS: A very strong sense of urgency always seems to be stressed by those who work in research, especially by those whose work has a direct impact on the future of medicine. What dangers do our current lack of understanding regarding the unanswered questions within your field pose us? Why is this type of work so vital?

SCR: Currently, there are more and more people in the world who live longer, and it is expected that in the years to come older individuals on the planet will outnumber the young ones. We do not know, however, whether the increased life expectancy will be accompanied by health and productivity or by disease. Age is a risk factor for many non-communicable or chronic disorders such as neurodegenerative diseases, cardiovascular diseases and cancer. Therefore, I think that it is important to understand the mechanisms that underlie aging and age-related conditions in order to be able to develop novel treatments and improve the health of the elderly.

SS: For you personally, what is the most rewarding aspect of working in science?

SCR: Although making new discoveries in an exciting field of research feels rewarding, what I find most gratifying in science is to see students in the classroom and young researchers in the lab becoming inspired to pursue careers in science.

SS: If you were to give one piece of advice to incoming freshmen that are considering a career in research science, what would that be?

SCR: My advice is: get involved in research as early as you can but most importantly be passionate about your work and perseverant toward your goals!

The JOSHUA staff would like to thank Dr. Chtarbanova-Rudloff for her time and wish her the best in her research. Roll Tide!

Selected Publications:

Kounatidis I*, Chtarbanova S*, Cao Y, Hayne M, Jayanth D, Ganetzky B & Ligoxygakis P. NF-κB immunity in the brain determines fly lifespan in healthy ageing and age-related neurodegeneration. Cell Rep. 2017 Apr 25;19(4):836-848. *Equal contribution.

Katzenberger RJ, Chtarbanova S, Rimkus SA, Fischer JA, Kaur G, Seppala JM, Swanson LC, Zajac JE, Ganetzky B & Wassarman DA. Death following traumatic brain injury in Drosophila is associated with intestinal barrier dysfunction (2015). eLife. 10.7554/eLife.04790

Chtarbanova S, Lamiable O, Lee KZ, Galiana D, Troxler L, Meignin C, Hetru C, Hoffmann JA, Daeffler L & Imler JL. Drosophila C virus systemic infection leads to intestinal obstruction (2014). J Virol. Sep 24. pii: JVI.02320-14. Article selected as a JVI Spotlight Feature.

Cao Y*, Chtarbanova S*, Petersen AJ & Ganetzky B. Dnr1 mutations cause neurodegeneration in Drosophila by activating the innate immune response in the brain (2013). Proc Natl Acad Sci U S A. May 7; 110 (19): E1752-60. * Equal contribution. Article selected by the Faculty of 1000.

Chtarbanova S & Imler JL. Microbial sensing by Toll receptors: a historical perspective (2011). Review. Arterioscler Thromb Vasc Biol. Aug; 31(8): 1734 8.

Eleftherianos I, Won S, Chtarbanova S, Squiban B, Ocorr K, Bodmer R, Beutler B,Hoffmann JA & Imler JL. ATP-sensitive potassium channel (K(ATP))-dependent regulation of cardiotropic viral infections (2011). Proc Natl Acad Sci U S A. Jul 19; 08 (29): 12024-9.

JOSHUA was made possible by the following organizations:

University of Alabama
Office of the President

Tri-Beta National Honor Society
Kappa Beta Chapter

Howard Hughes Medical Institute

National Science Foundation

Computer Based Honors Program

And by the 2016-2017 JOSHUA Editing Staff

2018 Submission Guidelines

We accept articles from current undergraduate students at The University of Alabama (UA). If you are a graduate student or recent alumnus of UA, we will consider your article if the majority of your work was conducted while you were an undergraduate at UA. Undergraduate students from other institutions may submit; however, priority will be given to those who conducted their research at UA.

1. Your name, e-mail address, and phone number must be included.

2. Your submission must relate to science or health.

3. Your work must be sponsored by a faculty member.

4. The length of your submission must be between 2000 and 4500 words. We will accept longer submissions if the author can limit the submission to the required length for the publication, and any extra material is able to be published online.

5. Figures, charts, and graphs are allowed but not required. (Note: The color will be mostly black and white.)

6. Your paper must contain an abstract.

7. Your citations must follow the guidelines listed on our website at joshua.ua.edu

8. The deadline for submission is February 12, 2018.

9. E-mail submissions to joshua.alabama@gmail.com

To access previous editions of JOSHUA or to learn more about contributing to the journal, please visit us online at

http://joshua.ua.edu/


SHELBY HALL

THE UNIVERSITY OF ALABAMA®